metals

MDPI

Article

The ESTPHAD Concept: An Optimised Set of Simplified Equations to Estimate the Equilibrium Liquidus and Solidus Temperatures, Partition Ratios and Liquidus Slopes for Quick Access to Equilibrium Data in Solidification Software Part III: Ternary Eutectic-Type Equilibrium Phase Diagram

Gergely Kőrösy [1], András Roósz [1,2,*], Ádám Végh [1] and Tamás Mende [1]

[1] Institute of Physical Metallurgy, Metal Forming and Nanotechnology, Faculty of Materials and Chemical Engineering, University of Miskolc, 3515 Miskolc, Hungary
[2] HUN-REN TKI, Materials Science Research Group, 3515 Miskolc, Hungary
* Correspondence: andras.roosz@uni-miskolc.hu

Abstract

The liquidus and solidus temperatures, the initial temperature of the solidification of binary eutectics, and the partition ratios of the solid solution at the Al corner of the ternary eutectic-type Al-Si-Cu alloy system were calculated using the thermodynamically based ESTPHAD method. It is shown that these data can be calculated from the liquidus and solidus data of the two binary equilibrium phase diagrams (first estimation), the binary phase diagram and the eutectic valleys in the ternary system (second estimation), as well as the binary phase diagram, the eutectic valleys, and one (third estimation) and more (fourth estimation) liquidus and solidus temperatures of the ternary equilibrium phase diagram with varying precisions. A database calculated with Thermo-Calc software (version 4.1.0.4995), was used for the calculations.

Keywords: liquidus and solidus temperature; partition ratio; binary and ternary eutectic-type equilibrium phase diagram; Al-Cu-Si alloy system

Check for updates

Academic Editor: Changming Fang

Received: 10 November 2025
Revised: 2 January 2026
Accepted: 8 January 2026
Published: 11 January 2026

Copyright: © 2026 by the authors. Licensee MDPI, Basel, Switzerland. This article is an open access article distributed under the terms and conditions of the Creative Commons Attribution (CC BY) license.

1. Introduction

For researchers of materials science and engineering, one of the most important types of information is knowing which phases are present in a material system at given values of state variables (temperature, pressure, concentrations) and whether they deal with metallic alloys, ceramics, salts, polymers, or organic compounds. This information is provided by the so-called equilibrium phase diagram (EPD).

The equilibrium of phases in thermodynamic terms is when it is true for all the constituents of each phase that the chemical potentials (μ, partial molar free energies) are equal. Equilibrium can refer to the total mass of phases or only to the interface of the phases; the diagrams constructed based on the latter are the restricted equilibrium phase diagrams [1,2].

In an EPD, the areas (binary EPDs) or volume parts (ternary, quaternary, etc., EPDs) in which different phases are located are separated by lines (binary EPDs) and two-dimensional or multi-dimensional surfaces (ternary, quaternary, etc., EPDs). Crossing lines or surfaces, the number of phases increases or decreases by one because of a phase transition. These phase

transformations are extremely important in various industrial technologies (e.g., mould and continuous casting, heat treatment).

The experimental determination of EPDs began in the second half of the 19th century, when the necessary technical conditions (e.g., thermocouples for temperature measurement, sample preparation technologies for microstructure analysis, and suitable light microscopes) were required. The real boom was brought about by the development of differential thermal analysis (DTA, DSC) and the widespread adoption of the X-ray diffraction technique.

2. Calculation of the EPD

Based on the EPDs, the concentration of the phases in equilibrium with each other, the proportion of mass of the phases, and the temperature of the beginning and end of the phase transformation can be determined.

As long as EPDs were only used to determine transformation temperatures in technology design (e.g., liquidus temperature in casting practice, $\alpha \leftrightarrow \gamma$ start and end temperatures of transformation in the heat treatment of steels), it was sufficient to determine the necessary data from graphically existing EPDs. However, the data determined in this way were not too accurate, and the reading error could easily have been as high as ± 10 K, which could have made the design of the technology uncertain. Therefore, the development of the theory of phase transformation processes (e.g., solidification and solid phase transformations) has necessitated the computation of data.

Until the introduction of the Calculation of Phase Diagram (CALPHAD) calculation model [3] and the software based on it (Thermo-Calc, FactSage), EPDs were only available as diagrams created from the processing of measurement results. In the solidification and solid phase transformation calculations, the lines representing the starting and ending temperatures of the transformation (liquidus, solidus, major, minor) as a function of concentration were approximated with straight lines (binary EPDs [4,5]) and surfaces (ternary, quaternary EPDs) with planes or polynomials. The regression functions for calculating the liquidus temperature and the partition ratio are a simple polynomial without any thermodynamic background in the case of aluminium alloys [6–9], steels [10–12], ceramics [13], and salts [14].

2.1. The CALPHAD Method

The basis of the CALPHAD method is that the free energy functions G of the phases occurring in the measured phase diagram are constructed as a function of temperature and concentrations [15–18]. In the case of a binary system, for a solid (s) and liquid (l) solution in equilibrium with each other

$$G = G_A X_A + G_B X_B + X_A X_B \Omega + RT(X_A lnX_A + X_B lnX_B) \quad (1)$$

Some data of the functions are known from measurements (e.g., the free energy functions of pure constituents or compounds), but not the Ω describing the interaction of the elements. By deriving the G functions, the partial free energy functions of the phases in equilibrium can be given by deriving the G functions:

$$\mu_A^l = G_A^l + RTlnX_A^l + X_B^l \Omega^l \text{ and } \mu_A^s = G_A^s + RT\ lnX_A^s + X_B^s \Omega^s \quad (2)$$

and

$$\mu_B^l = G_B^l + RTlnX_B^l + X_A^l \Omega^l \text{ and } \mu_B^s = G_B^s + RT\ lnX_B^s + X_A^s \Omega^s \quad (3)$$

According to the Gibbs condition mentioned above, the partial molar free energies must be equal:

$$G_A^l + RTlnX_A^l + X_B^l\Omega^l = G_A^s + RTlnX_A^s + X_B^s\Omega^s \quad (4)$$

and

$$G_B^l + RTlnX_B^s + X_A^l\Omega^l = G_B^s + RTlnX_B^s + X_A^s\Omega^s \quad (5)$$

In the case of systems with three or more components, the equations are, of course, significantly more complicated.

$G_A^l, G_A^s, G_B^l, G_B^s$, are known at a given temperature. The temperature-dependent can be determined by iteration using the EPD data obtained from the measurement. The knowledge of these can be used to calculate the concentration of the phases (e.g., liquid and solid) that maintain equilibrium with each other at a given temperature. It follows from the above that the CALPHAD method also leads to reliable results only if the EPD based on the measurements is known. During the simulation of a transformation process, the concentration of phases in equilibrium is determined in each step with a CHALPHAD-type software. Thus, the authors of some of the most recent works have utilised the CALPHAD calculation of thermodynamic data for simulating macrosegregation [19,20], microsegregation [21], the mushy zone [22], and solid phase transformation [23]. Several authors have found that this method is not very efficient, as it is especially time-consuming for three- or multi-component alloys, where the time required for CALPHAD-type calculations is lengthy, and the concentrations of each finite element must be recalculated multiple times within a single time step [20,23–25]. Two methods have been developed to solve the problem. The first step in both methods is to create a temperature-concentration map using CALPHAD-type software. In the case of the mapping method [26–28], the temperature corresponding to the two (binary system) or four (ternary system) closest concentrations to the given concentration is searched, and then between them, the temperature corresponding to the given concentration is determined. In the case of the other method, a polynomial is created through regression; however, these polynomials do not have a thermodynamic basis [6,7,29,30].

2.2. The ESTHAD Method

In the two earlier papers, we showed the use of the ESTPHAD method in the case of Si-Ge isomorphous and Al-Si [31], Al-Mg eutectic-type binary, and Ag-Au-Pd isomorphous ternary [32] EPDs. Most of the practically used ternary aluminium alloys are eutectic-type (e.g., Al-Mg-Si, Al-Mg-Cu, Al-Mg-Zn, Al-Cu-Mg, Al-Mn-Si, Al-Mn-Fe). In this paper, the usability of the ESTPHAD method is demonstrated in the Al corner of the Al-Si-Cu eutectic type TEPD.

The basis of the ESTHAD method is the same as that of CALPHAD, with the difference that the effect between the elements is not taken into account when writing free energy functions, because the aim is not to give functions that can be used to directly calculate the concentration of the phases holding equilibrium with each other, but "only" to determine the form of the equations of the curves (binary system) or surfaces (ternary, quaternary systems) that give the starting and ending temperature of the transformation at given concentration(s).

The details of the construction of the equations used in the case of the ternary Ag-Au-Pd system are shown in [32]. In this paper, we present the equations used to calculate the liquidus (T_L) and solidus temperatures (T_s), the start temperature of solidification of the binary eutectics (T_{BE}), the slopes of the liquidus (M), and the partition ratios (k) in the case of the Al-Si-Cu eutectic-type ternary equilibrium phase system.

The aim of the paper—in addition to showing the calculation of the liquidus and solidus surfaces at the Al corner of the Al-Si-Cu ternary equilibrium phase diagram with the Estphad system—is to show that it is possible to obtain information of limited accuracy about the liquidus and solidus temperature of the ternary system, as well as about the partition ratios, even if only the binary systems that make up the ternary system and certain elements of the ternary system are known (e.g., eutectic valleys data, some liquidus and solidus temperature data). A further aim was to show how the accuracy of the calculation depends on the amount of data in the available liquidus and solidus temperatures of the ternary system.

2.2.1. The Liquidus (T_L) and Solidus (T_s) Temperatures

The thermodynamic derivation of the T_L and *Ts* functions was presented in [32].

$$T_L\left(X^l_{Si}, X^l_{Cu}\right) = T_{Al} / \left[F^l_{AlSi}\left(X^l_{Si}\right) + F^l_{AlCu}\left(X^l_{Cu}\right) + \Delta F^l_{AlSiCu}\left(X^l_{Si}, X^l_{Cu}\right) + 1\right] \quad (6)$$

$$F^l_{AlSi}\left(X^l_{Si}\right) = A^l_{AlSi}(1,0)X^l_{Si} + A^l_{AlSi}(2,0)\left(X^l_{Si}\right)^2 + A^l_{ASi}(3,0)\left(X^l_{Si}\right)^3 + \quad (7)$$

$$F^l_{AlCu}\left(X^l_{Cu}\right) = A^l_{AlCu}(0,1)X^l_{Cu} + A^l_{AlCu}(0,2)\left(X^l_{Cu}\right)^2 + A^l_{AlCu}(0,3)\left(X^l_{Cu}\right)^3 + \quad (8)$$

$$\Delta F^l_{AlSiCu}\left(X^l_{Si}, X^l_{Cu}\right) = A^l_{AlSiCu}(1,1)X^l_{Si}X^l_{Cu} + A^l_{AlSiCu}(1,2)X^l_{Si}\left(X^l_{Cu}\right)^2 + A^l_{AlSiCu}(2,1)\left(X^l_{si}\right)^2 X^l_{Cu} + \quad (9)$$

$$T_s(X^s_{Si}, X^s_{Cu}) = T_{Al} / [F^s_{AlSi}(X^s_{Si}) + F^s_{AlCu}(X^s_{Cu}) + \Delta F^s_{AlSiCu}(X^s_{Si}, X^s_{Cu}) + 1] \quad (10)$$

where

$$F^s_{AlSi}(X^s_{Si}) = A^s_{AlSi}(1,0)X^s_{Si} + A^s_{AlSi}(2,0)(X^s_{Si})^2 + A^s_{AlSi}(3,0)(X^s_{Si})^3 + \quad (11)$$

$$F^s_{AlCu}(X^s_{Cu}) = A^s_{AlCu}(0,1)X^s_{Cu} + A^s_{AlCu}(0,2)(X^s_{Cu})^2 + A^s_{AlCu}(0,3)(X^s_{Cu})^3 + \ldots \quad (12)$$

$$\Delta F^s_{AlSiCu}(X^s_{Si}, X^s_{Cu}) = A^s_{AlSiCu}(1,1)X^s_{Si}X^s_{Cu} + A^s_{AlSiCu}(1,2)X^s_{Si}\left(X^s_{Cu}\right)^2 + A^s_{AlSiCu}(2,1)(X^s_{si})^2 X^s_{Cu} + \quad (13)$$

2.2.2. The Beginning Temperature of the Solidification of the Binary Eutectics (T_{BE})

If the concentration of the alloy is greater than the maximum solubility of the solid solution, the solidification of the solid solution is followed by the solidification of a binary and then a ternary eutectic. The solidification of the binary eutectic lasts from the starting temperature of T_{BE} to the temperature of the ternary eutectic *(T_{TE}).* Two types of binary eutectic solidified depending on the concentrations: α+Si or α+Al_2Cu.

In this case, the partition ratios (and, thus, tie lines) are known for both experimentally determined and calculated TEPD with CHALPHAD-type software. Tie lines form the surface of the beginning of the solidification of binary eutectics. According to the theory, tie lines meet at the corner point only if the solidified phase is a pure element (pure Cu or Si). In this case, the slope of the tie lines *(M_{BE})* can be defined, which is equal to X^l_{Si}/X^l_{Cu} or X^l_{Cu}/X^l_{Si}. Knowing these, the $T_{BE}(M_{BE})$ function can be determined. Substituting the X^l_{Si}/X^l_{Cu} or X^l_{Cu}/X^l_{Si} value of the alloy or into the function gives the initial temperature of the solidification of the binary eutectic. If the tie lines do not meet at the corner point, the average slope can be determined:

$M^{aver}_{BE} = (X^l_{Si}/X^l_{Cu} + X^s_{Si}/X^s_{Cu})/2$ or $M^{aver}_{BE} = (X^l_{Cu}/X^l_{Si} + X^s_{Cu}/X^s_{Si})/2$ depending on the type of eutectics. If $X^l_{Si}/X^l_{Cu} \approx X^s_{Si}/X^s_{Cu}$ the error will be acceptable.

2.2.3. The Slopes of the Liquidus Surface

The slopes of the liquid surface can be calculated as a partial derivative of the function of liquidus temperature ($T_L\left(X^l_{Si}, X^l_{Cu}\right)$) :

$$M^{Si}_{AlSiCu}\left(X^l_{Si}, X^l_{Cu} = const\right) = \frac{\partial T_L}{\partial X^l_{Si}} = \frac{T_{Al}\frac{\partial\left(1+F^l_{AlSi}\left(X^l_{Si}\right)+\Delta F^l_{AlSiCu}\left(X^l_{Si,}X^l_{Cu}\right)\right)}{\partial X^l_{Si}}}{\left(1+F^l_{AlSiCu}\left(X^l_{Si}, X^l_{Cu}\right)\right)^2} = \frac{T_A S^{Si}_{AlSiCu}\left(X^l_{Si}, X^l_{Cu} = const\right)}{\left(1+F^l_{AlSiCu}\left(X^l_{Si}, X^l_{Cu}\right)\right)^2} \quad (14)$$

$$M^{Si}_{AlSiCu}\left(X^l_{Si} = const, X^l_{Cu}\right) = \frac{\partial T_L}{\partial X^l_{Cu}} = \frac{T_{Al}\frac{\partial\left(1+F^l_{AlCu}\left(X^l_{Cu}\right)+\Delta F^l_{AlSiCu}\left(X^l_{Si,}X^l_{Cu}\right)\right)}{\partial X^l_{Cu}}}{\left(1+F^l_{AlSiCu}\left(X^l_{Si}, X^l_{Cu}\right)\right)^2} = \frac{T_{Al} S^{Cu}_{AlSiCu}\left(X^l_{si} = const, X^l_{Cu}\right)}{\left(1+F^l_{AlSiCu}\left(X^l_{Si}, X^l_{Cu}\right)\right)^2} \quad (15)$$

2.2.4. The Partition Ratios (k^{AlSiCu}_{Si} and k^{AlSiCu}_{Cu})

If we calculate the constants of the equations from data obtained using CALPHAD, then the approximation method employed in the previous article is not necessary to calculate partition ratios, because the concentrations of liquidus and solids are known to be in equilibrium. For equation derivation, see [31,32].

$$lnk^{AlSiCu}_{Si}\left(X^l_{Si}, X^l_{Cu}\right) = lnk^{AlSi}_{Si}\left(X^l_{Si}\right) + \Delta lnk^{AlSiCu}_{Si}\left(X^l_{Si}, X^l_{Cu}\right) \quad (16)$$

$$k^{AlSiCu}_{Si}\left(X^l_{Si}, X^l_{Cu}\right) = \exp\left(lnk^{Alsi}_{Si}\left(X^l_{Si}\right) + \Delta lnk^{AlSiCu}_{si}\left(X^l_{Si}, X^l_{Cu}\right)\right) \quad (17)$$

$$lnk^{AlSiCu}_{Cu}\left(X^l_{Si}, X^l_{Cu}\right) = lnk^{AlCu}_{Cu}\left(X^l_{Cu}\right) + \Delta lnk^{AlSiCu}_{Cu}\left(X^l_{Si}, X^l_{Cu}\right) \quad (18)$$

$$k^{AlSiCu}_{Cu}\left(X^l_{Si}, X^l_{Cu}\right) = \exp\left(lnk^{Alsi}_{Cu}\left(X^l_{Cu}\right) + \Delta lnk^{AlSiCu}_{Cu}\left(X^l_{Si}, X^l_{Cu}\right)\right) \quad (19)$$

where

$$lnk^{AlSi}_{Si}\left(X^l_{Si}\right) = B^l_{AlSi}(0,0) + B^l_{AlSi}(1,0)\left(X^l_{Si}\right)^1 + B^l_{AlSi}(2,0)\left(X^l_{Si}\right)^2 + B^l_{AlSi}(3,0)\left(X^l_{Si}\right)^3 + \quad (20)$$

$$lnk^{AlCu}_{Cu}\left(X^l_{Cu}\right) = B^l_{AlCu}(0,0) + B^l_{AlCu}(1,0)\left(X^l_{Cu}\right)^1 + B^l_{AlCu}(2,0)\left(X^l_{Cu}\right)^2 + B^l_{AlCu}(3,0)\left(X^l_{Cu}\right)^3 \quad (21)$$

and

$$\begin{gathered}\Delta lnk^{AlSiCu}_{Si}\left(X^l_{Si}, X^l_{Cu}\right) = B^l_{AlSiCu}(0,1)\left(X^l_{Si}\right)^0 X^l_{Cu} + B^l_{AlSiCu}(0,2)\left(X^l_{Si}\right)^0\left(X^l_{Cu}\right)^2 + \\ B^l_{AlSiCu}(0,3)\left(X^l_{Si}\right)^0\left(X^l_{Cu}\right)^3 + + B^l_{AlSiCu}(1,1)X^l_{Si}X^l_{Cu} + B^l_{AlSiCu}(2,1)\left(X^l_{Si}\right)^2 X^l_{Cu} + B^l_{AlSiCu}(1,2)X^l_{Si}\left(X^l_{Cu}\right)^2 +\end{gathered} \quad (22)$$

$$\begin{gathered}\Delta lnk^{AlSiCu}_{Cu}\left(X^l_{Si}, X^l_{Cu}\right) = C^l_{AlSiCu}(0,1)\left(X^l_{Cu}\right)^0 X^l_{Si} + C^l_{AlSiCu}(0,2)\left(X^l_{Cu}\right)^0\left(X^l_{Si}\right)^2 \\ C^l_{AlSiCu}(0,3)\left(X^l_{Cu}\right)^0\left(X^l_{Si}\right)^3 + + C^l_{AlSiCu}(1,1)X^l_{Si}X^l_{Cu} + C^l_{AlSiCu}(2,1)\left(X^l_{Si}\right)^2 X^l_{Cu} + C^l_{AlSiCu}(1,2)X^l_{Si}\left(X^l_{Cu}\right)^2\end{gathered} \quad (23)$$

3. Calculation of the Constants

3.1. Calculation of the Constants of Liquidus and Solidus Functions

A database from a CALPHAD-type calculation was used to calculate the constants. Using the Thermo-Calc software (version 4.1.0.4995), the equilibrium concentrations of the liquid and solid phases of Si and Cu were calculated at 14 isotherms as the Cu concentration changed in 0.001 mol fraction steps. The mol fraction was changed to wt% because it is used in practice.

3.1.1. First Estimation (Only the Al-Si and Al-Cu BEPD Are Known)

Calculation of the $F^l_{AlSi}\left(X^l_{Si}\right), F^l_{AlCu}\left(X^l_{Cu}\right)$ and $F^s_{AlSi}(X^s_{Si}), F^s_{AlCu}(X^s_{Cu})$ maps:

$$F^l_{AlSi}\left(X^l_{Si}\right) = \frac{T_{Al}}{T^l_{AlSi}(X^l_{si})} - 1 \text{ and } F^s_{AlSi}(X^s_{Si}) = \frac{T_{Al}}{T^s_{AlSi}(X^s_{Si})} - 1 \quad (24)$$

and

$$F^l_{AlCu}\left(X^l_{Cu}\right) = \frac{T_{Al}}{T^l_{AlCu}(X^l_{Cu})} - 1 \text{ and } F^s_{AlCu}(X^s_{Cu}) = \frac{T_{Al}}{T^s_{AlCu}(X^s_{Cu})} - 1 \quad (25)$$

Used these two maps, the constant of the $\boldsymbol{F^l_{AlSi}}\left(X^l_{Si}\right)$, $\boldsymbol{F^l_{AlCu}}\left(X^l_{Cu}\right)$ and $\boldsymbol{F^s_{AlSi}}(X^s_{Si})$, $\boldsymbol{F^s_{AlCu}}(X^s_{Cu})$ functions was calculate by regression. The determined constants can be seen in Table 1 (liquidus), Table 2 (solidus), Table 3 (liquidus), Table 4 (solidus), Table 5 (liquidus) and Table 6 (solidus), (first row: Al-Si, first column: Al-Cu BEPD).

The liquidus and the solidus temperatures are

$$T_L = T_{Al}/(\boldsymbol{F^l_{AlSi}}\left(X^l_{Si}\right) + \boldsymbol{F^l_{AlCu}}\left(X^l_{Cu}\right) + 1) \quad (26)$$

and

$$T_s = T_{Al}/(\boldsymbol{F^s_{AlSi}}(X^s_{Si}) + \boldsymbol{F^s_{AlCu}}(X^s_{Cu}) + 1) \quad (27)$$

3.1.2. Second Estimation (The BEPDs and the Binary Eutectic Valleys Are Known)

In some cases, in addition to the BEPDs, only data of the binary eutectic valleys are known. In this case, from this data the $F^{l,\,eut}_{AlSiCu}\left(X^{l,eut}_{Si}, X^{l,eut}_{Cu}\right)$ and $F^{s,\,eut}_{AlSiCu}\left(X^{s,eut}_{Si}, X^{s,eut}_{Cu}\right)$ functions were calculated:

$$F^{l,eut}_{AlSiCu}\left(X^{\,l,eut}_{Si}, X^{l,eut}_{Cu}\right) = \frac{T_A}{T^{l,eut}_{AlSiCu}(X^{l,eut}_{si}, X^{l,eut}_{Cu})} - 1 = F^l_{AlSi}\left(X^l_{Si}\right) + F^l_{AlCu}\left(X^l_{Cu}\right) + \Delta F^{l,eut}_{AlSiCu}\left(X^{l,eut}_{Si}, X^{l,eut}_{Cu}\right) \quad (28)$$

and then

$$\Delta F^{l,eut}_{AlSiCu}\left(X^{l,eut}_{Si}, X^{l,eut}_{Cu}\right) = F^{l,eut}_{AlSiCu}\left(X^{l,eut}_{Si}, X^{l,eut}_{Cu}\right) - F^l_{AlSi}\left(X^l_{Si}\right) - F^l_{AlCu}\left(X^l_{Cu}\right) \quad (29)$$

$$F^{s,eut}_{AlSiCu}\left(X^{\,s,eut}_{Si}, X^{s,eut}_{Cu}\right) = \frac{T_A}{T^{lseut}_{AlSiCu}(X^{lseut}_{si}, X^{s,eut}_{Cu})} - 1 = F^s_{AlSi}(X^s_{Si}) + F^s_{AlCu}(X^s_{Cu}) + \Delta F^{s,eut}_{AlSiCu}\left(X^{s,eut}_{Si}, X^{s,eut}_{Cu}\right) \quad (30)$$

and then

$$\Delta F^{s,eut}_{AlSiCu}\left(X^{s,eut}_{Si}, X^{s,eut}_{Cu}\right) = F^{s,eut}_{AlSiCu}\left(X^{s,eut}_{Si}, X^{s,eut}_{Cu}\right) - F^s_{AlSi}(X^s_{Si}) - F^s_{AlCu}(X^s_{Cu}) \quad (31)$$

From the $\Delta F^{l,eut}_{AlSiCu}\left(X^{l,eut}_{Si}, X^{l,eut}_{Cu}\right)$ and $\Delta F^{s,eut}_{AlSiCu}\left(X^{s,eut}_{Si}, X^{s,eut}_{Cu}\right)$ data sets the constants of the $\Delta\boldsymbol{F^{l,eut}_{AlSiCu}}\left(X^{l,eut}_{Si}, X^{l,eut}_{Cu}\right)$ and $\Delta\boldsymbol{F^{s,eut}_{AlSiCu}}\left(X^{s,eut}_{Si}, X^{s,eut}_{Cu}\right)$ functions were calculated by regression (Tables 1 and 2).

Table 1. Liquidus temperature calculated from BEPDs and the eutectic valleys. Second estimation.

$\boldsymbol{T^l_{AlCuSi}}$	$(\boldsymbol{X^l_{Si}})^0$	$(\boldsymbol{X^l_{Si}})^1$	$(\boldsymbol{X^l_{Si}})^2$	$(\boldsymbol{X^l_{Si}})^3$	
$(\boldsymbol{X^l_{Cu}})^0$	0	0.006259277	9.09114E-05	2.84167E-06	Binary Al-Si
$(\boldsymbol{X^l_{Cu}})^1$	0.002928252	0.000146803	−2.54818E-06		
$(\boldsymbol{X^l_{Cu}})^2$	−5.17929E-06	5.40796E-06			
$(\boldsymbol{X^l_{Cu}})^3$	1.23057E-06	−7.59466E-08			
	Binary Al-Cu				

Table 2. Solidus temperature calculated from BEPDs and the eutectic valleys. Second estimation.

T^s_{AuCuSi}	$(X^s_{Si})^0$	$(X^s_{Si})^1$	$(X^s_{Si})^2$	
$(X^s_{Cu})^0$	0	0.062168995	0.000768388	Binary Al-Si
$(X^s_{Cu})^1$	0.027873196	0.001484473		
$(X^s_{Cu})^2$	3.59926E-05	−0.000763994		
$(X^s_{Cu})^3$	−0.000128955			
	Binary Al-Cu			

The liquidus and solidus temperatures of the TEPD are

$$T_L = T_{Al}/(\boldsymbol{F^l_{AlSi}}\left(X^l_{Si}\right) + \boldsymbol{F^l_{AlCu}}\left(X^l_{Cu}\right) + \Delta\boldsymbol{F^{l,eut}_{AlSiCu}}\left(X^{l,eut}_{Si}, X^{l,eut}_{Cu}\right) + 1) \quad (32)$$

and

$$T_s = T_{Al}/(\boldsymbol{F^s_{AlSi}}(X^s_{Si}) + \boldsymbol{F^s_{AlCu}}(X^s_{Cu}) + \Delta\boldsymbol{F^{s,eut}_{AlSiCu}}\left(X^{s,eut}_{Si}, X^{s,eut}_{Cu}\right) + 1) \quad (33)$$

3.1.3. Third and Fourth Estimations, if the BEPDs, the Binary Eutectic Valleys and Some Data Are Known on the Liquidus and Solidus Surfaces of the TEPD

In most cases, the TEPD are shown on the perpendicular projection with isotherms. In this case

In addition to the BEPDs, the data of the binary eutectic valleys and some liquidus and solidus temperatures (third estimation only one isotherm, fourth estimation 14 isotherms) are known. In this case, from this data the $F^l_{AlSiCu}\left(X^l_{Si}, X^l_{Cu}\right)$ and $F^s_{AlSiCu}(X^s_{Si}, X^s_{Cu})$ functions were calculated:

$$F^l_{AlSiCu}\left(X^{\,l}_{Si}, X^l_{Cu}\right) = \frac{T_A}{T^l_{AlSiCu}(X^l_{si}, X^l_{Cu})} - 1 = F^l_{AlSi}\left(X^l_{Si}\right) + F^l_{AlCu}\left(X^l_{Cu}\right) + \Delta F^l_{AlSiCu}\left(X^l_{Si}, X^l_{Cu}\right) \quad (34)$$

and then

$$\Delta F^l_{AlSiCu}\left(X^l_{Si}, X^l_{Cu}\right) = F^l_{AlSiCu}\left(X^l_{Si}, X^l_{Cu}\right) - F^l_{AlSi}\left(X^l_{Si}\right) - F^l_{AlCu}\left(X^l_{Cu}\right) \quad (35)$$

$$F^{s,eut}_{AlSiCu}(X^{\,s}_{Si}, X^s_{Cu}) = \frac{T_A}{T^s_{AlSiCu}(X^s_{si}, X^s_{Cu})} - 1 = F^s_{AlSi}(X^s_{Si}) + F^s_{AlCu}(X^s_{Cu}) + \Delta F^s_{AlSiCu}(X^s_{Si}, X^s_{Cu}) \quad (36)$$

and then

$$\Delta F^s_{AlSiCu}(X^s_{Si}, X^s_{Cu}) = F^s_{AlSiCu}(X^s_{Si}, X^s_{Cu}) - F^s_{AlSi}(X^s_{Si}) - F^s_{AlCu}(X^s_{Cu}) \quad (37)$$

From the $\Delta F^l_{AlSiCu}\left(X^l_{Si}, X^l_{Cu}\right)$ and $\Delta F^s_{AlSiCu}(X^s_{Si}, X^s_{Cu})$ data sets, the constants of the $\Delta\boldsymbol{F^l_{AlSiCu}}\left(X^l_{Si}, X^l_{Cu}\right)$ and $\Delta\boldsymbol{F^s_{AlSiCu}}(X^s_{Si}, X^s_{Cu})$ functions were calculated by regression (Third estimation: Table 3. liquidus, Table 4. solidus, fourth estimation: Table 5. liquidus, Table 6, solidus).

Table 3. Liquidus temperature calculated from BEPDs, eutectic valleys and one (830 K) isotherm. Third estimation.

T^l_{AlCuSi}	$(X^l_{Si})^0$	$(X^l_{Si})^1$	$(X^l_{Si})^2$	$(X^l_{Si})^3$	
$(X^l_{Cu})^0$	0	0.006259277	9.09114E-05	2.84167E-06	Binary Al-Si
$(X^l_{Cu})^1$	0.002928252	5.5654E-05	5.9301E-06		
$(X^l_{Cu})^2$	−5.17929E-06	5.22492E-06			
$(X^l_{Cu})^3$	1.23057E-06				
	Binary Al-Cu				

Table 4. Solidus temperature calculated from BEPDs, eutectic valleys and one (830 K) isotherm. Third estimation.

T^s_{AuCuSi}	$(X^s_{Si})^0$	$(X^l_{Si})^s$	$(X^s_{Si})^2$	
$(X^s_{Cu})^0$	0	0.062168995	0.000768388	Binary Al-Si
$(X^s_{Cu})^1$	0.027873196	0.003036506	−0.001081166	
$(X^s_{Cu})^2$	3.59926E-05	−0.000898423		
$(X^s_{Cu})^3$	−0.000128955			
	Binary Al-Cu			

Table 5. Liquidus temperature calculated from BEPDs, eutectic valleys and all isotherms. Fourth estimation.

T^l_{AuCuSi}	$(X^l_{Si})^0$	$(X^l_{Si})^1$	$(X^l_{Si})^2$	$(X^l_{Si})^3$	
$(X^l_{Cu})^0$	0	0.006259277	9.09114E-05	2.84167E-06	Binary Al-Cu
$(X^l_{Cu})^1$	0.002928252	6.1245E-05	5.76923E-06		
$(X^l_{Cu})^2$	−5.17929E-06	4.92776E-06			
$(X^l_{Cu})^3$	1.23057E-06				
	Binary Al-Si				

Table 6. Solidus temperature calculated from BEPDs, eutectic valleys and all isotherms. Fourth estimation.

T^s_{AuCuSi}	$(X^s_{Si})^0$	$(X^s_{Si})^1$	$(X^s_{Si})^2$	
$(X^s_{Cu})^0$	0	0.062168995	0.000768388	Binary Al-Si
$(X^s_{Cu})^1$	0.027873196	0.002143483	−0.000655231	
$(X^s_{Cu})^2$	3.59926E-05	−0.000687929		
$(X^s_{Cu})^3$	−0.000128955			
	Binary Al-Cu			

The liquidus and solidus temperatures of the TEPD are

$$T_L = T_{Al}/(\boldsymbol{F^l_{AlSi}}\left(X^l_{Si}\right) + \boldsymbol{F^l_{AlCu}}\left(X^l_{Cu}\right) + \Delta\boldsymbol{F^l_{AlSiCu}}\left(X^{l,eut}_{Si}, X^{l,eut}_{Cu}\right) + 1) \quad (38)$$

and

$$T_s = T_{Al}/(\boldsymbol{F^s_{AlSi}}(X^s_{Si}) + \boldsymbol{F^s_{AlCu}}(X^s_{Cu}) + \Delta\boldsymbol{F^s_{AlSiCu}}\left(X^{s,eut}_{Si}, X^{s,eut}_{Cu}\right) + 1) \quad (39)$$

3.1.4. Calculation of Constants of the Beginning Temperature Function ($T_{BE}(M_{BE})$) of Solidification of Binary Eutectics

As mentioned in Section 2.2.2, two different binary eutectics solidify when the concentration of the alloy is greater than the maximum solubility of the solid solution. The tie lines at the solidification of the binary eutectics are known both from calculation or measuring. Determined that the slope of the tie lines versus temperature can be obtained a function with which the beginning temperature of the solidification of binary eutectics can be calculated. The details of the calculation are presented in the Section 4.

3.2. Calculation of the Constants of Liquidus Slopes

The M^{Si}_{AlSiCu} and M^{Cu}_{AlSiCu} liquidus slopes are the partition derivative of the $T_L\left(X^l_{Si}, X^l_{Cu}\right)$ function. Since the constants of the denominator of the functions are known, only the constants of the derivative of the numerator are shown below:

$$S^{Si}_{AlSiCu}\left(X^l_{Si}, X^l_{Cu} = const\right) = \frac{\partial}{X^l_{Si}} F^l_{AlSiCu}\left(X^l_{Si,} X^l_{Cu}\right) = A^l_{AlSi}(1,0) + 2A^l_{AlSi}(2,0)\left(X^l_{Si}\right)^1 + 3A^l_{ASi}(3,0)\left(X^l_{Si}\right)^2 + A^l_{AlSiCu}(1,1)X^l_{Cu} + A^l_{AlSiCu}(1,2)\left(X^l_{Cu}\right)^2 + 2A^l_{AlSiCu}(2,1)\left(X^l_{Si}\right)^1 X^l_{Cu} + \quad (40)$$

$$S^{Cu}_{AlSiCu}\left(X^l_{Si}, X^l_{Cu} = const\right) = \frac{\partial}{X^l_{Cu}} F^l_{AlSiCu}\left(X^l_{Si,} X^l_{Cu}\right) = A^l_{AlCu}(0,1) + 2A^l_{AlCu}(0,2)\left(X^l_{Cu}\right)^1 + 3A^l_{AlCu}(0,3)\left(X^l_{Cu}\right)^2 + A^l_{AlSiCu}(1,1)X^l_{Si} + 2A^l_{AlSiCu}(1,2)X^l_{Si}\left(X^l_{Cu}\right)^1 + A^l_{AlSiCu}(2,1)\left(X^l_{Si}\right)^2 + \quad (41)$$

The constants of the $S^{Si}_{AlSiCu}\left(X^l_{Si}, X^l_{Cu} = const\right)$ and $S^{Cu}_{AlSiCu}\left(X^l_{Si}, X^l_{Cu} = const\right)$ functions are in Tables 7 and 8 (fourth estimation of T_L). The first row of these Tables shows the constants in the case of BEPDs.

Table 7. The constants of the derivative of the numerator of $S^{Cu}_{AlSiCu}\left(X^l_{Si}, X^l_{Cu} = const\right)$ function calculated from BEPDs and the eutectic valleys. Fourth estimation of the liquidus temperatures.

S^{Cu}_{AlSiCu}	$\left(X^l_{Cu}\right)^0$	$\left(X^l_{Cu}\right)^1$	$\left(X^l_{Cu}\right)^2$	
$\left(X^l_{Si}\right)^0$	0.002928252	2 × −5.17929E-06	3 × 1.23057E-06	Binary Al-Cu
$\left(X^l_{Si}\right)^1$	5.5654E-05	2 × 5.22492E-06		
$\left(X^l_{Si}\right)^2$	5.9301E-06			

Table 8. The constants of the derivative of the numerator of $S^{Si}_{AlSiCu}\left(X^l_{Si}, X^l_{Cu} = const\right)$ function calculated from all data. Fourth estimation of the liquidus temperatures.

S^{Si}_{AlSiCu}	$\left(X^l_{Si}\right)^0$	$\left(X^l_{Si}\right)^1$	$\left(X^l_{Si}\right)^2$	
$\left(X^l_{Cu}\right)^0$	0.006259277	2 × 9.09114E-05	3 × 2.84167E-06	Binary Al-Si
$\left(X^l_{Cu}\right)^1$	5.5654E-05	2 × 5.9301E-06		
$\left(X^l_{Cu}\right)^2$	5.22492E-06			

3.3. Calculation of the Constants of Partition Ratios Functions

As it was mentioned in Section 3.1. the equilibrium Si and Cu concentrations were calculated by Thermo-Calc, so the k_{Si} and k_{Cu} were calculable directly from the X^l_{Si}, X^s_{Si} and X^l_{Cu}, X^s_{Cu} concentration pairs:

$$k_{Si} = X^s_{Si}/X^l_{Si},\ k_{Cu} = X^s_{Cu}/X^l_{Cu} \text{ and } X^s_{Si} = X^l_{Si}k_{Si},\ X^s_{Cu} = X^l_{Cu}k_{Cu} \quad (42)$$

3.3.1. First Estimation

Similarly to the liquidus and solidus temperature, only the *Al-Si* and *Al-Cu* BEPD data were used to determine the partition ratios map. The B^l_{AlSi} and B^l_{AlCu} constants of the $\boldsymbol{lnk^{AlSi}_{Si}}\left(X^l_{Si}\right)$ and $\boldsymbol{lnk^{AlCu}_{Cu}}\left(X^l_{Cu}\right)$ functions were determined by regression ($\boldsymbol{lnk^{AlCu}_{Cu}}$ first row in Table 9, $\boldsymbol{lnk^{AlSi}_{Si}}$ first row in Table 10, $\boldsymbol{lnk^{AlCu}_{Cu}}$ first row in Table 11 and $\boldsymbol{lnk^{AlSi}_{Si}}$ first row in Table 12).

Table 9. $\boldsymbol{lnk^l_{Si}}$ calculated from BEPDs and eutectic valleys. Second estimation.

$\boldsymbol{lnk^l_{Si}}$	$\left(X^l_{Si}\right)^0$	$\left(X^l_{Si}\right)^1$	$\left(X^l_{Si}\right)^2$	$\left(X^l_{Si}\right)^3$
$\left(X^l_{Cu}\right)^0$	−2.288892406	0.01197891	0.00032586	Binary Al-Si
$\left(X^l_{Cu}\right)^1$	0.005118707	0.000448357	−2.20231E-06	
$\left(X^l_{Cu}\right)^2$	0.00035785			

Table 10. lnk_{Cu}^{l} calculated from BEPDs and eutectic valleys. Second estimation.

lnk_{Cu}^{AlSiCu}	$(X_{Cu}^{l})^{0}$	$(X_{Cu}^{l})^{1}$	$(X_{Cu}^{l})^{2}$	
$(X_{Si}^{l})^{0}$	−2.280465486	−2.25824E-05	0.000453888	Binary Al-Cu
$(X_{Si}^{l})^{1}$	0.043426906	0.0002552	2.50114E-06	
$(X_{Si}^{l})^{2}$	−0.002892515			

Table 11. lnk_{Si}^{l} calculated from BEPDs, eutectic valleys and all isotherms. Fourth estimation.

lnk_{Si}^{AlSiCu}	$(X_{Si}^{l})^{0}$	$(X_{Si}^{l})^{1}$	$(X_{Si}^{l})^{2}$	$(X_{Si}^{l})^{3}$
$(X_{Cu}^{l})^{0}$	−2.288892406	0.01197891	0.00032586	Binary Al-Si
$(X_{Cu}^{l})^{1}$	0.005118707	0.000448357	−2.20231E-06	
$(X_{Cu}^{l})^{2}$	0.00035785			

Table 12. lnk_{Cu}^{l} calculated from BEPDs, eutectic valleys and all isotherms. Fourth estimation.

lnk_{Cu}^{AlSiCu}	$(X_{Cu}^{l})^{0}$	$(X_{Cu}^{l})^{1}$	$(X_{Cu}^{l})^{2}$	
$(X_{Si}^{l})^{0}$	−2.280465486	−2.25824E-05	0.000453888	Binary Al-Cu
$(X_{Si}^{l})^{1}$	0.022447756	−6.438E-05	2.63906E-05	
$(X_{Si}^{l})^{2}$	−0.001012122			

3.3.2. Second Estimation

The partition coefficients were determined from the BEPDs partition ratios and the concentration pairs of the eutectic valleys.

This calculation version is interesting because, in the case of graphical TEPD, only these tie lines are known in TEPDs.

$$k_{Si}^{AlSiCu}\left(X_{Si}^{l,eut}, X_{Cu}^{l,\,eut}\right) = X_{Si}^{s,eut}/X_{Si}^{l,eut} \text{ and } k_{Cu}^{AlSiCu}\left(X_{Si}^{l,eut}, X_{Cu}^{l,\,eut}\right) = X_{Cu}^{s,eut}/X_{Cu}^{l,eut} \quad (43)$$

$$lnk_{Si}^{AlSiCu}\left(X_{Si}^{l,eut}, X_{Cu}^{l,\,eut}\right) = lnk_{Si}^{AlSi}\left(X_{Si}^{l}\right) + \Delta lnk_{Si}^{AlSiCu}\left(X_{Si}^{l,eut}, X_{Cu}^{l,eut}\right) \quad (44)$$

$$\Delta lnk_{Si}^{AlSiCu}\left(X_{Si}^{l,eut}, X_{Cu}^{l,\,eut}\right) = lnk_{Si}^{AlSiCu}\left(X_{Si}^{l,eut}, X_{Cu}^{l,eut}\right) - lnk_{Si}^{AlSi}\left(X_{Si}^{l}\right) \quad (45)$$

and

$$lnk_{Cu}^{AlSiCu}\left(X_{Si}^{l,eut}, X_{Cu}^{l,\,eut}\right) = lnk_{Cu}^{AlSi}\left(X_{Cu}^{l}\right) + \Delta lnk_{Cu}^{AlSiCu}\left(X_{Si}^{l,eut}, X_{Cu}^{l,eut}\right) \quad (46)$$

$$\Delta lnk_{Cu}^{AlSiCu}\left(X_{Si}^{l,eut}, X_{Cu}^{l,\,eut}\right) = lnk_{Cu}^{AlSiCu}\left(X_{Si}^{l,eut}, X_{Cu}^{l,eut}\right) - lnk_{Cu}^{AlSi}\left(X_{Cu}^{l}\right) \quad (47)$$

The constants of $\Delta \boldsymbol{lnk_{Si}^{AlSiCu}}\left(X_{Si}^{l,eut}, X_{Cu}^{l,\,eut}\right)$ and $\Delta \boldsymbol{lnk_{Cu}^{AlSiCu}}\left(X_{Si}^{l,eut}, X_{Cu}^{l,\,eut}\right)$ function were determined by regression, and are in Table 9 ($\boldsymbol{lnk_{Si}^{AlSiCu}}$) and in Table 10 ($\boldsymbol{lnk_{Cu}^{AlSiCu}}$).

3.3.3. Third Estimation

In this case, the tie lines are known in the BEPDs, the eutectic valleys and between the liquidus and solidus surfaces (isotherms).

$$k_{Si}^{AlSiCu}\left(X_{Si}^{l}, X_{Cu}^{l,}\right) = X_{Si}^{s}/X_{Si}^{l} \text{and } k_{Cu}^{AlSiCu}\left(X_{Si}^{l}, X_{Cu}^{l,}\right) = X_{Cu}^{s}/X_{Cu}^{l} \quad (48)$$

$$lnk_{Si}^{AlSiCu}\left(X_{Si}^{l}, X_{Cu}^{l}\right) = lnk_{Si}^{AlSi}\left(X_{Si}^{l}\right) + \Delta lnk_{Si}^{AlSiCu}\left(X_{Si}^{l}, X_{Cu}^{l}\right) \quad (49)$$

$$\Delta lnk_{Si}^{AlSiCu}\left(X_{Si}^{l}, X_{Cu}^{l}\right) = lnk_{Si}^{AlSiCu}\left(X_{Si}^{l}, X_{Cu}^{l}\right) - lnk_{Si}^{AlSi}\left(X_{Si}^{l}\right) \quad (50)$$

and

$$lnk_{Cu}^{AlSiCu}\left(X_{Si}^{l}, X_{Cu}^{l}\right) = lnk_{Cu}^{AlSi}\left(X_{Cu}^{l}\right) + \Delta lnk_{Cu}^{AlSiCu}\left(X_{Si}^{l}, X_{Cu}^{l}\right) \quad (51)$$

$$\Delta lnk_{Cu}^{AlSiCu}\left(X_{Si}^{l}, X_{Cu}^{l}\right) = lnk_{Cu}^{AlSiCu}\left(X_{Si}^{l}, X_{Cu}^{l}\right) - lnk_{Cu}^{AlSi}\left(X_{Si}^{l}\right) \quad (52)$$

The constants of $\Delta \boldsymbol{lnk_{Si}^{AlSiCu}}\left(X_{Si}^{l,eut}, X_{Cu}^{l,\,eut}\right)$ and $\Delta \boldsymbol{lnk_{Cu}^{AlSiCu}}\left(X_{Si}^{l,eut}, X_{Cu}^{l,\,eut}\right)$ function were determined by regression, and are in Tables 11 and 12.

4. Results

4.1. Liquidus and Solidus Isotherms

4.1.1. First Estimation

Knowing the liquidus and solidus functions of BEPDs, the liquidus and solidus isotherms of the Al-Si-Cu TEPD were calculated, assuming that the interaction effect of the Si and Cu in the liquid and solid phases are negligible, i.e., $\Delta \boldsymbol{F_{AlSiCu}^{l}}\left(X_{Si}^{l}, X_{Cu}^{l}\right) = 0$ and $\Delta \boldsymbol{F_{AlSiCu}^{s}}\left(X_{Si}^{s}, X_{Cu}^{s}\right) = 0$. The calculated liquidus and the solidus of the Al-Si and Al-Cu BEPDs are shown in Figures 1a and 2a, respectively. Figures 1b and 2b show the difference (DELTA T) between the results of Thermo-Calc and ESTPHAD calculations. Using the two BEPD functions, the liquidus (Equation (27)) and solidus (Equation (28)) temperatures of the TEPD can be calculated. The calculated liquidus and solidus isotherms in the Al corner are shown in Figures 3a and 4a. Figures 3b and 4b show the temperature difference (DELTA T) between the Thermo-Calc and the ESTPHAD calculations along the isotherms as a function of Cu concentration.

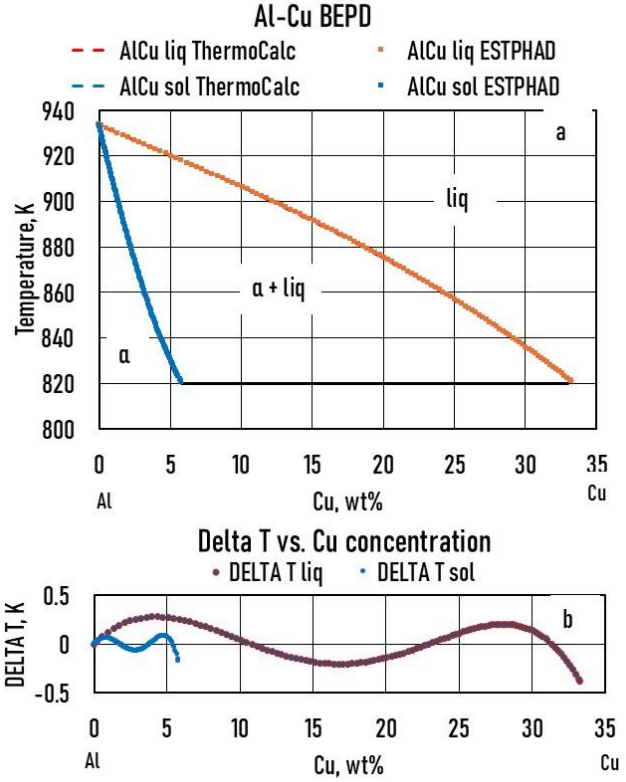


Figure 1. (**a**): the liquidus (red line) and solidus (blue line) of Al-Cu BEPD calculated by Thermo-Calc (solid line) and ESTPHAD (markers). (**b**): the difference (DELTA T) between the two calculations.

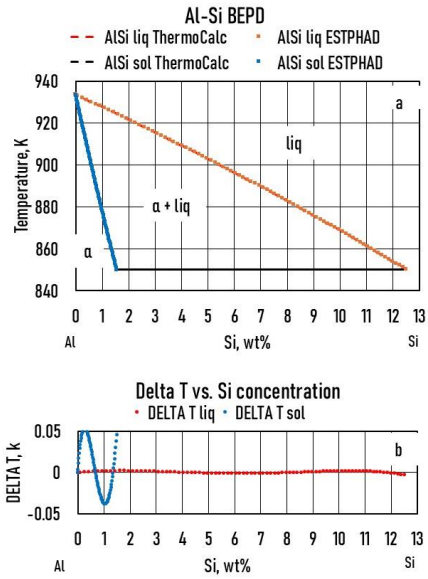


Figure 2. (**a**): liquidus (red line) and the solidus (blue line) of Al-Si BEPD calculated by Thermo-Calc (solid line) and ESTPHAD (markers). (**b**): the difference (DELTA T) between the two calculations.

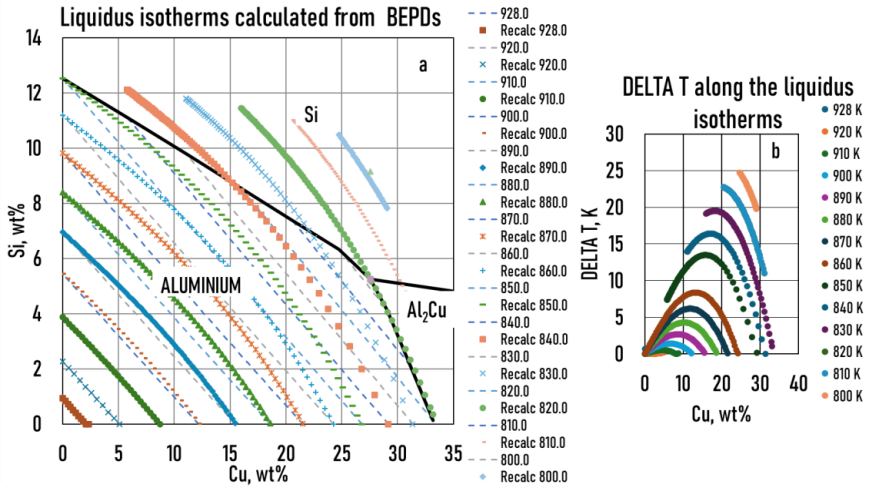


Figure 3. (**a**): first estimation of liquidus isotherms. (**b**): temperature difference (DELTA T) between the Thermo-Calc and the ESTPHAD calculations along the isotherms.

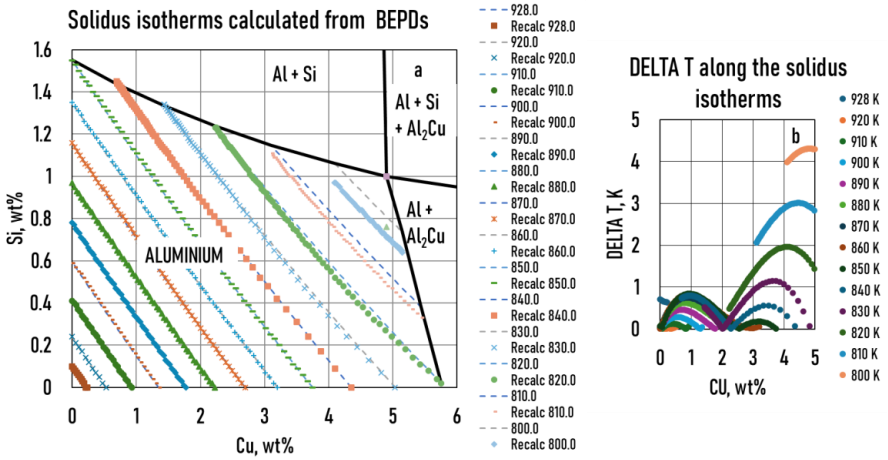


Figure 4. (**a**): first estimation of solidus isotherms. (**b**): temperature difference (DELTA T) between the Thermo-Calc and the ESTPHAD calculations along the isotherms.

4.1.2. Second Estimation

In many cases, only data from BEPDs and the concentration pairs of eutectic valleys are known. In these cases, the data of the eutectic valleys can also be used to calculate the liquidus (Equation (33)) and solidus (Equation (34)) temperatures more accurately than the first estimation. The calculated liquidus and solidus isotherms in the Al corner are shown in Figures 5a and 6a. Figures 5b and 6b show the temperature difference (DELTA T) between the Thermo-Calc and the ESTPHAD calculations along the isotherms as a function of the Cu concentration.

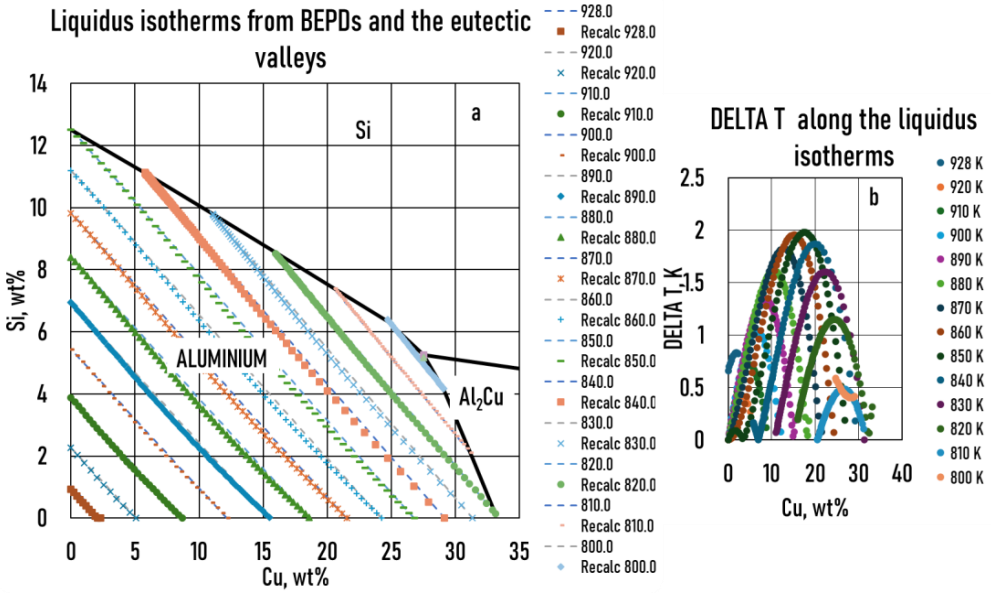


Figure 5. (**a**): second estimation of liquidus isotherms. (**b**): temperature difference (DELTA T) between the Thermo-Calc and the ESTPHAD calculations along the isotherms.

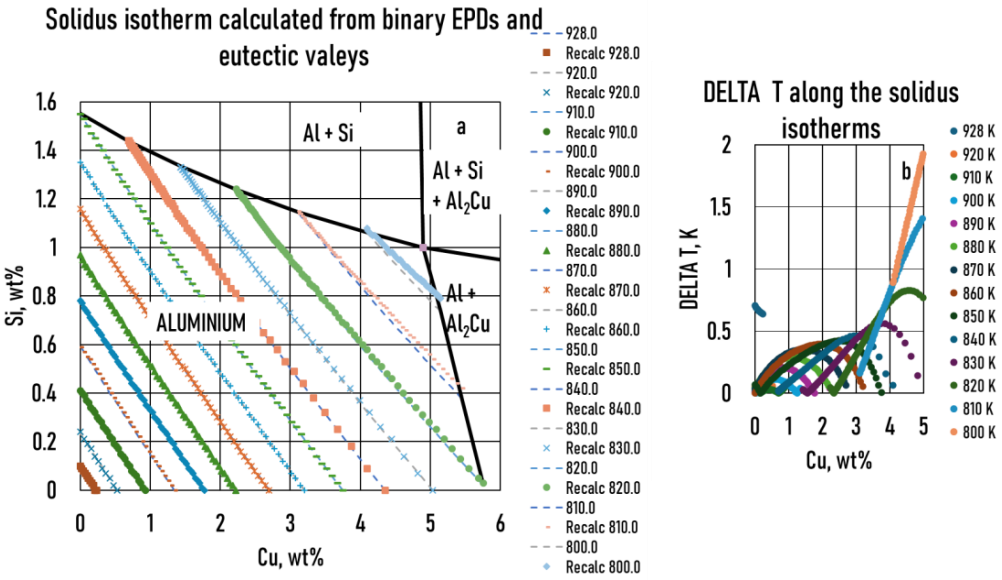


Figure 6. (**a**): second estimation of solidus isotherms. (**b**): temperature difference (DELTA T) between the Thermo-Calc and the ESTPHAD calculations along the isotherms.

4.1.3. Third and Fourth Estimation

In the case of measured TEBD diagrams, some measured liquidus and solidus temperatures, or some isotherms, on the surface of the liquidus and solidus are known. In the case of Thermo-Calc calculations, some isotherms on both surfaces are also known. The amount of data affects

the accuracy of the calculation. To examine the impact of data number, calculations were made using the data of the BEPDs, the eutectic valleys and the 1, 2, 3, 4, 5, and 14 (all) isotherms. The temperature, the number of isotherms, and the number of data used in the calculations are shown in Table 13. The calculation was made with Equations (39) and (40). The calculated liquidus and solidus isotherms, using the data of BEPDs, the eutectic valleys, and one isotherm (850 K), are shown in Figures 7a and 8a (third estimation) and when all data of 14 isotherms were used in Figures 9a and 10a (fourth estimation). The temperature difference (DELTA T) between the Thermo-Calc and the ESTPHAD calculations along the isotherms is shown in Figures 7b and 8b (third estimation), Figures 9b and 10b (fourth estimation) in the case of liquidus and solidus, respectively.

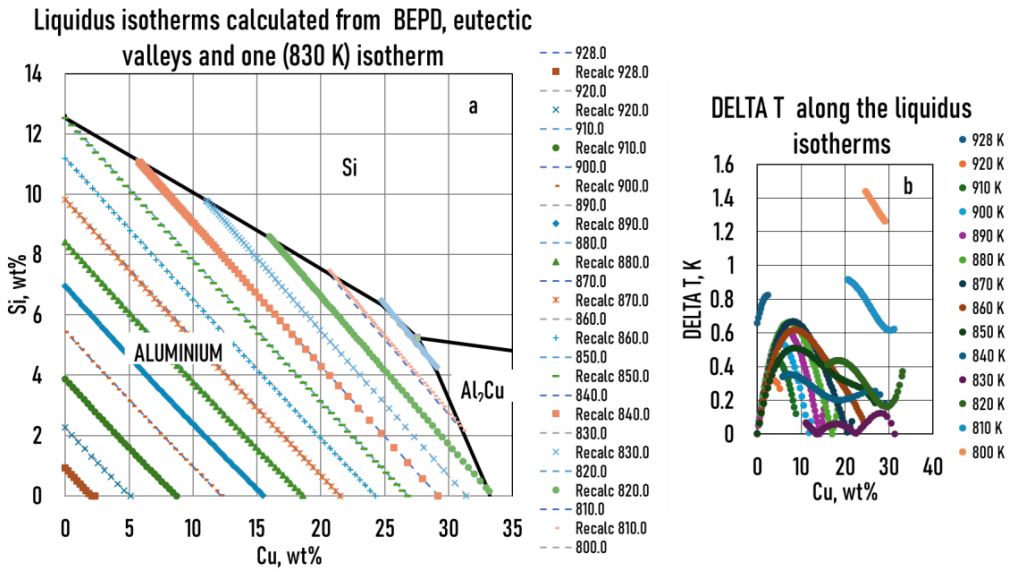


Figure 7. (**a**): third estimation of liquidus isotherms calculated with one (830 K) isotherm. (**b**): temperature difference (DELTA T) between the Thermo-Calc and the ESTPHAD calculations along the isotherms.

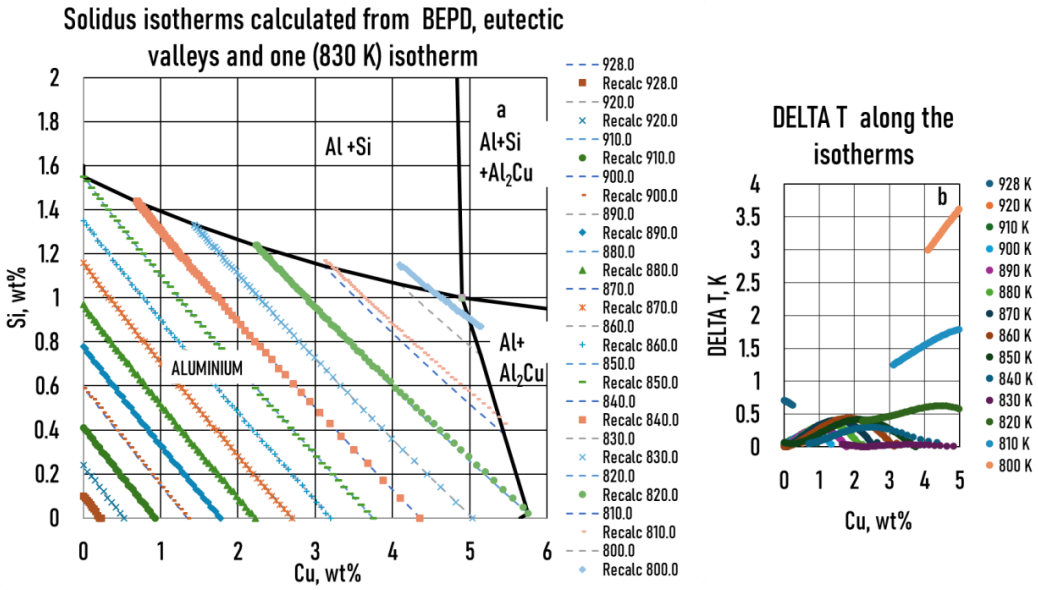


Figure 8. (**a**): third estimation of solidus isotherms calculated with one (830 K) isotherm. (**b**): temperature difference (DELTA T) between the Thermo-Calc and the ESTPHAD calculations along the isotherms.

Table 13. Number and the data of the isotherms in the calculation.

	Third and Fourth Estimation							Second Estimation	First Estimation
	Number of isotherms								
Temperature, K	14	7	5	4	3	2	1		
928	X	X	X	X	X	X			
920	X								
910	X	X							
900	X		X						
890	X	X		X					
880	X				X				
870	X	X	X						
860	X								
850	X	X		X					
840	X		X						
830	X	X			X	X	X		
820	X								
810	X	X	X	X					
800	X								
Sum data of isotherm	722	349	254	194	74	75	63		
Eut. valley data	10	10	10	10	10	10	10	10	
Al-Cu data	123	123	123	123	123	123	123	123	123
Al-Si data	83	83	83	83	83	83	83	83	83
Sum	938	565	470	410	354	291	279	216	206
DELTA T*, K liq	0.083	0.088	0.087	0.09	0.12	0.126	0.128	0.79	8.96
DELTA T*, K sol	0.147	0.15	0.175	0.18	0.22	0.23	0.23	0.35	0.94

DELTA T^*_{aver} the difference between all the data calculated by ESTPHAD and ThermoCalc.

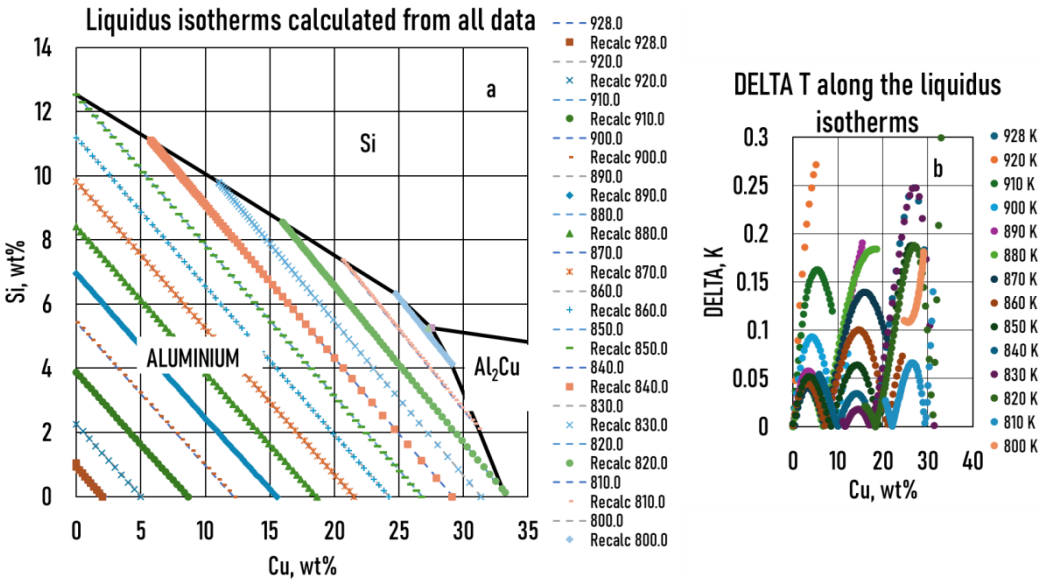


Figure 9. (**a**): fourth estimation of liquidus isotherms calculated with all isotherms. (**b**): temperature difference (DELTA T) between the Thermo-Calc and the ESTPHAD calculations along the isotherms.

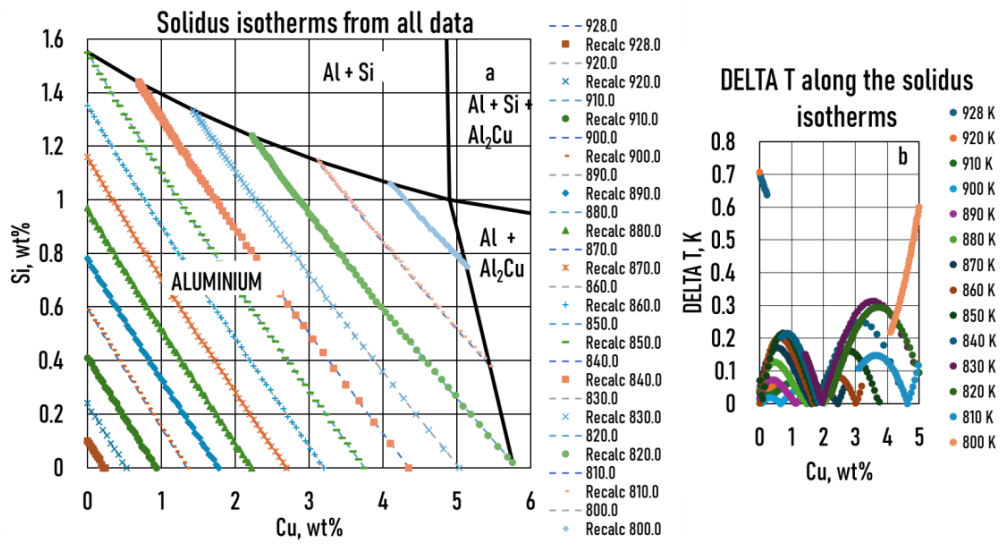


Figure 10. (**a**): fourth estimation of solidus isotherms calculated with all isotherms. (**b**): temperature difference (DELTA T) between the Thermo-Calc and the ESTPHAD calculations along the isotherms.

In the ternary diagrams and the tables DELTA T and DELTA Si, Cu mean the absolute values!!

4.2. The Beginning Temperature of the Solidification of Binary Eutectics

The surface of the solidification of the two eutectics is separated by the valley (tie line) of the ternary eutectic, above which the Al+Si eutectic and below the Al+Al_2Cu eutectic solidify. The calculation of the slope must be chosen so that at zero concentration (BEPD), its value is not infinite, but zero. Therefore, values were calculated above the ternary eutectic valley X^{l}_{Cu}/X^{l}_{Si} and below it X^{l}_{Si}/X^{l}_{Cu} (Table 14). The values of the X^{s}_{Cu}/X^{s}_{Si} and X^{s}_{Si}/X^{s}_{Cu} were calculated too, which were practically the same as the values of X^{l}_{Cu}/X^{l}_{Si} and X^{l}_{Si}/X^{l}_{Cu}. Consequently, the tie lines meet at the corner point. Using these data, the constants of two $T_{BE}(M_{TB})$ functions were determined by regression as follows:

Above the ternary eutectic valley:

$$T_{BE} = 1.9097{M_{BE}}^2 - 19.944M_{BE} + 850.08 \quad (53)$$

Below the ternary eutectic valley:

$$T_{BE} = 3787.4{M_{BE}}^3 - 663.43{M_{BE}}^2 - 126.27M_{BE} + 820.46 \quad (54)$$

Table 14. The slope of the tie lines of binary eutectics.

M_{BE}	T, K
X^{l}_{Cu}/X^{l}_{Si}	
0	850
0.519474	840
1.128312	830
1.868701	819
2.780053	809
3.904228	801
5.245714	798.5
X^{l}_{Si}/X^{l}_{Cu}	
0.19	798.5
0.142	800
0.068	810
0	820

At the simulation of the solidification the $X_{Si}(X_{Cu})$ functions of the binary eutectic valleys are interesting, so these were calculated:

$$X_{Si}(X_{Cu}) = -0.0006{X_{Cu}}^2 - 0.2422X_{Cu} + 12.563 \text{ at } \alpha + \text{Si binary eutectic} \quad (55)$$

$$X_{Si}(X_{Cu}) = -0.0025{X_{Cu}}^2 - 0.8534X_{Cu} + 31.082 \text{ at } \alpha + Al_2Cu \text{ binary eutectic} \quad (56)$$

The tie lines calculated by the ESTPAD and Thermo-Calc, and the comparison of the results of calculations is shown in Figure 11.

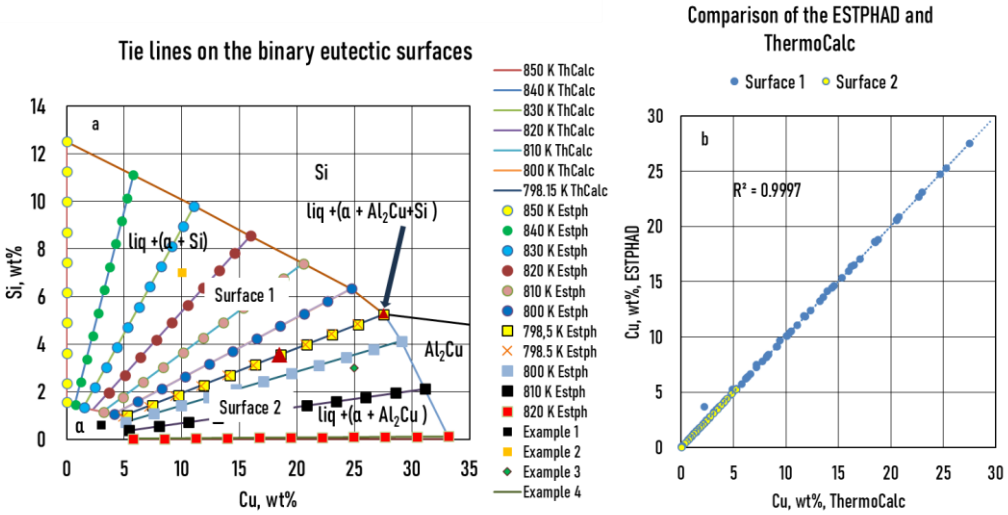


Figure 11. (**a**): calculated tie lines by Thermo-Calc and ESTPHAD. (**b**): comparison of the tie lines calculated by Thermo-Calc and ESTPHAD.

4.3. The Liquidus Slopes

During the simulation of solidification, it is often necessary to calculate the slopes of the liquidus surface. Tables 7 and 8 contain the constants of the numerators $S^{Si}_{AlSiCu}\left(X^l_{Si},\ X^l_{Cu} = const\right)$ and $S^{Cu}_{AlSiCu}\left(X^l_{Si},\ X^l_{Cu} = const\right)$ of the slope functions (M^{Si}_{AlSiCu} and M^{Cu}_{AlSiCu}) calculated from the fourth estimation of liquidus temperature used all isotherms. Figure 12a,b shows the values of the slope functions M^{Si}_{AlSiCu} and M^{Cu}_{AlSiCu} as a function of Cu and Si concentration along the given isotherm, respectively.

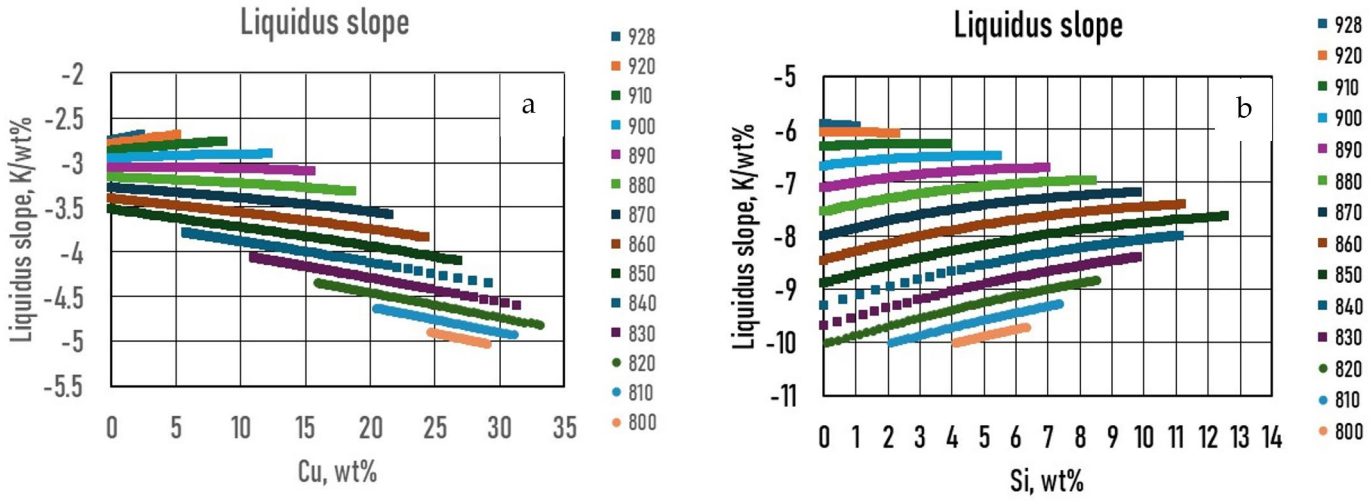


Figure 12. (**a**): $\partial T_L/\partial X_{Si}$ vs. Cu concentration. (**b**): $\partial T_L/\partial X_{Cu}$ vs. Si concentration.

4.4. Recalculation of the Solidus Isotherm from the Liquidus Isotherms Using the Partition Ratios

The aim of this recalculation was to determine those alloy concentrations in which we can obtain an acceptable solidus concentration using Equation (43). During the recalculation, the solidus concentrations were recalculated from the fourth estimated liquidus concentrations using the partition ratios along the liquidus isotherms. To compare the isotherms calculated by Equation (34) and the recalculated isotherms, the DELTA Cu and DELTA Si were determined (see Figure 13). Using recalculated concentrations, recalculated isotherms were constructed (Figures 14a, 15a and 16a). To study the change in DELTA Cu and DELTA Si along the isotherms, the DELTA Si versus DELTA Cu is shown in Figures 14b, 15b and 16b.

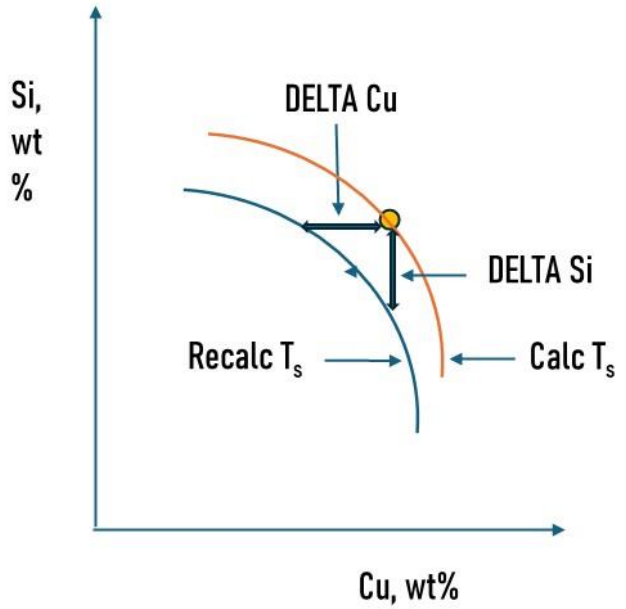


Figure 13. Method of the determination of DELTA Cu and DELTA Si.

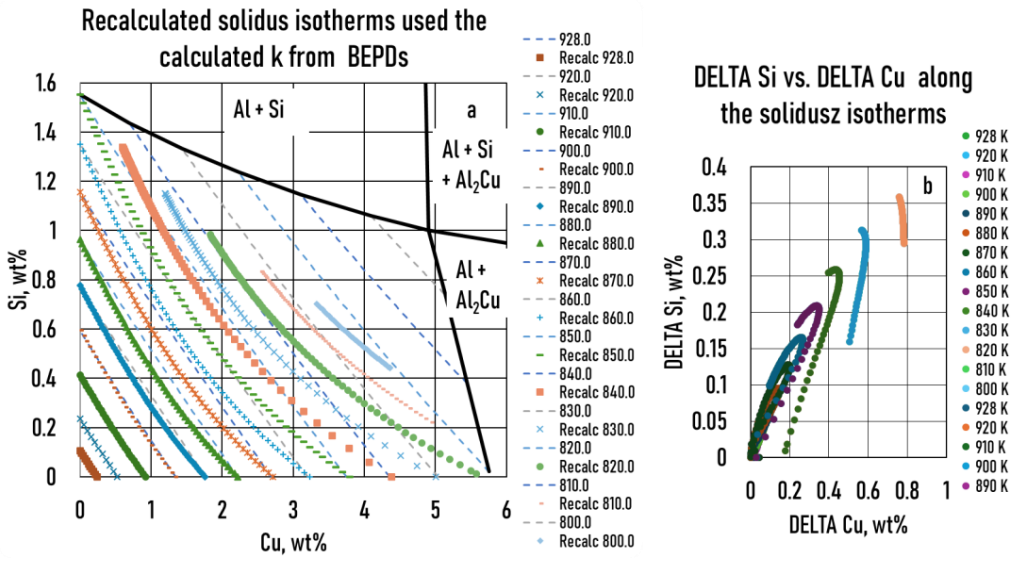


Figure 14. (**a**): recalculated solidus isotherms used the calculated partition ratios from BEPD. (**b**): DELTA Si concentration versus DELTA Cu concentration along the isotherms.

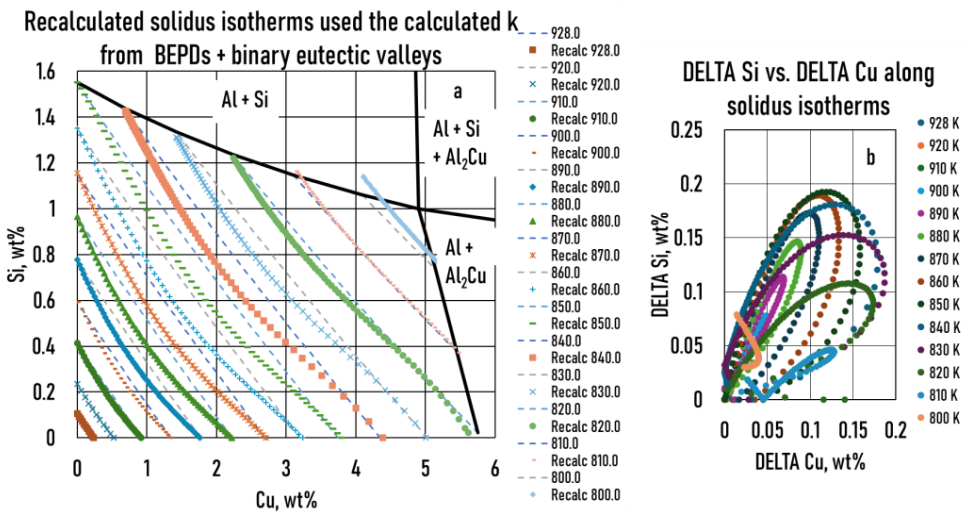


Figure 15. (**a**): recalculated solidus isotherms used the calculated partition ratios from BEPD and the binary eutectic valleys. (**b**): DELTA Si concentration versus DELTA Cu concentration along the isotherms.

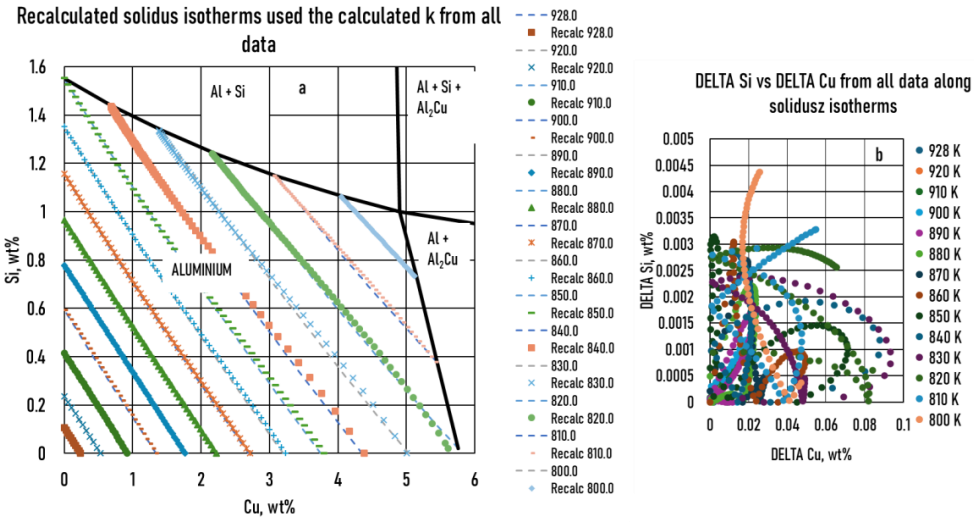


Figure 16. (**a**): recalculated solidus isotherms used the calculated partition ratios from BEPD, the binary eutectic valleys, and all isotherms. (**b**): DELTA Si concentration versus DELTA Cu concentration along the isotherms.

4.4.1. First Estimation

The partition ratios of the TEPD were estimated based on the partition ratios of the BEPDs. The concentration of the solidus isotherms was recalculated using these two partition ratios from the concentration of the liquidus isotherms along the isotherms. The solidus isotherms using the recalculated concentration are compared with the solidus isotherms calculated by the fourth estimation (Figure 14).

4.4.2. Second Estimation

The partition ratios of the TEPD were calculated using the partition ratios of the BEPDs and the partition ratios calculated from the tie lines of binary eutectic valleys. The concentration of the solidus isotherms was recalculated with these two partition ratios from the concentration of liquidus isotherms along the isotherms. The solidus isotherms using the recalculated concentration are compared with the solidus isotherms calculated by the fourth estimation (Figure 15).

4.4.3. Third Estimation

Using the partition ratios of the BEPDs, as well as the partition ratios of binary eutectic valleys and the calculated partition ratios derived from the data of all isotherms, the partition ratios were determined. The concentration of the solidus isotherms was recalculated with these two partition ratios from the concentration of liquidus isotherms. The recalculated solidus isotherms are compared with the calculated solidus isotherms calculated by the fourth estimation (Figure 16).

5. Discussion

5.1. Calculation of Liquidus and Solidus of BEPD

The ESTPHAD calculation approximates the results of Thermo-Calc with ±0.5 K (liquidus) and 0.1 K (solidus) in the case of Al-Cu BEPD, while with ±0.005 K (liquidus) and 0.05 K (solidus) in the case of Al-Si BEPD (Figure 1b (Al-Cu) and Figure 2b (Al-Si)).

5.2. Calculation of Liquidus and Solidus of TEPD

5.2.1. First Estimation

The constants of the T_L and T_s functions were calculated based on only the data from the BEPS (Equations (27) and (28)). Along the liquidus isotherms (Figure 3a), DELTA T is continuously changing between two T_{min} as a function of Cu concentration (Figure 3b). For isotherms starting at Al-Si BEPD (X_{Cu} = 0) and ending at Al-Cu BEPD (X_{Si} = 0) (between 928 K and 850 K), the DELTA T_{min} is determined by the BEPDs data, which are very small (see Section 5.1). Under 850 K DELTA T_{min} is at the Al-Cu BEPD. At the first isotherm (928 K), DELTA T_{max} and DELTA T_{aver} are near the same, 0.82 K and 0.73 K, and higher than at the second isotherm (920 K), 0.27 K and 0.17 K. As the temperature decreases, DELTA T_{max} and DELTA T_{aver} increase. DELTA T_{max} and DELTA T_{aver} under 910 K and 900 K are smaller by 1 K, and then in the concentration range under these isotherms, the first estimation is suitable for solidification simulation. Naturally, DELTA T_{max} is higher than DELTA T_{aver} (Appendix A, Figure 17).

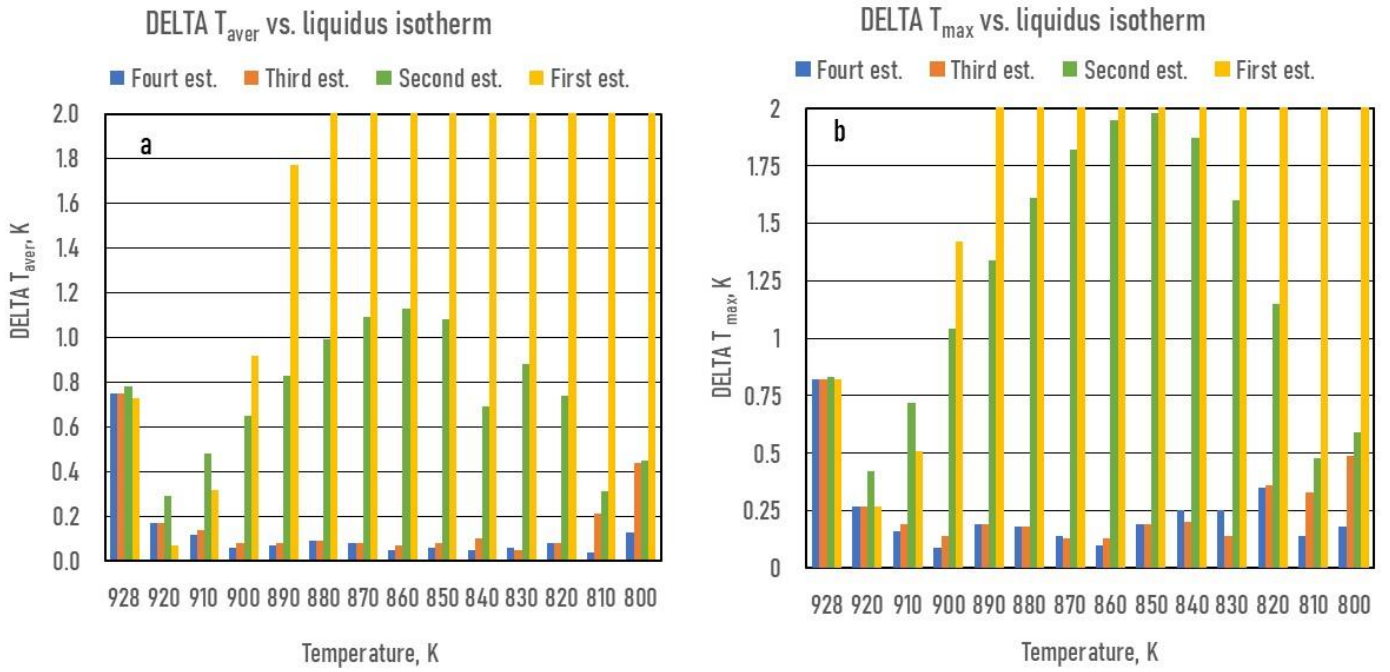


Figure 17. The liquidus temperature difference between the Thermo-Calc and ESTPHAD calculations at four different estimations as a function of the isotherm temperatures. (**a**): average, (**b**): maximum.

Along the solidus isotherms (Figure 4a), DELTA T is continuously changing between two DELTA T_{min} as a function of Cu concentration (Figure 4b). Like the liquidus isotherms, for isotherms starting at Al-Si BEPD (X_{Cu} = 0) and ending at Al-Cu BEPD (X_{Si} = 0) (between 928 K and 850 K), the DELTA T_{min} is determined by the BEPDs data, which are very small (see Section 5.1). From 840 K to 820 K, the isotherms start from the Al+Si binary eutectic valley and end at the Al-Cu BEPD, while at 810 K and 800 K, the isotherms are between the two binary valleys. At the first isotherm (928 K), DELTA T_{max} and DELTA T_{aver} are near the same, 0.7 K and 0.66 K, and higher than at the second isotherm (920 K), 0.06 K and 0.02 K. As the temperature decreases, DELTA T_{max} and DELTA T_{aver} increase from 0.06 K to 4.31 K and from 0.02 K to 4.23 K, respectively. DELTA T_{max} and DELTA T_{aver} remain smaller than 1 K until 840 K and 830 K, respectively (Appendix B, Figure 18).

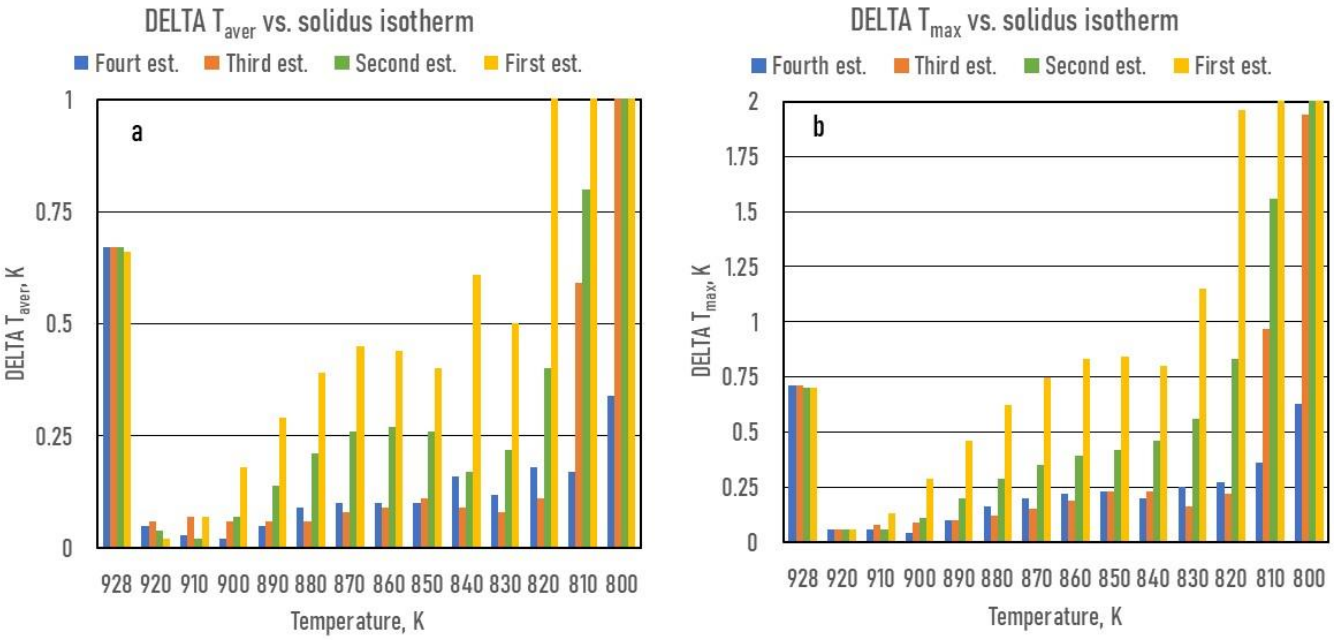


Figure 18. The solidus temperature difference between the Thermo-Calc and ESTPHAD calculations at four different estimations as a function of the isotherm temperatures. (**a**): average, (**b**): maximum.

5.2.2. Second Estimation

The constants of the T_L and T_s functions were calculated based on the data of the BEPDs and the data of the two binary eutectic valleys. Along the liquidus isotherms (Figure 5a), as in the first estimation, the DELTA T changes between two T_{min} as a function of Cu concentration (Figure 5b). The difference between the second and first estimations is that all isotherms begin at Al-Si BEPDs or the Al+Si eutectic valley and end at the Al-Cu BEPD or the Al+Al_2Cu eutectic valley, for which the DELTA T is very small. At the first isotherm (928 K), DELTA Tmax and DELTA T_{aver} are near the same in the two types of estimations, 0.83 K and 0.78 K, and higher than at the second isotherm (920 K), 0.42 K and 0.29 K. The DELTA T_{max} and DELTA T_{aver} continuously increase with decreasing temperature; the DELTA T_{max} is less than ~1 K to 900 K, but it does not exceed 2 K, while DELTA T_{aver} remains less than ~1 K throughout the entire range of the isotherms. (Appendix A, Figure 17).

In the case of solidus isotherms (Figure 6a), the DELTA T_{max} and DELTA T_{aver} vary similarly to that of liquidus isotherms (Figure 6b). The DELTA T_{max} and DELTA T_{aver} continuously increase with decreasing temperature. DELTA T_{max} is less than 1 K until 820 K, and DELTA T_{aver} until 810 K. At the ternary eutectic point, those are 2.1 K and 1.6 K (Appendix B, Figure 18).

5.2.3. Third and Fourth Estimations

The constants of the T_L and T_s functions were calculated based on the data of the BEPDs, the data of the two binary eutectic valleys, and some isotherms (from 1 to 14). From this calculation, two of them (the third estimation, calculated with only 830 K isotherm (Figure 7a, liquidus, Figure 8a, solidus), and the fourth estimation, with 14 isotherms (Figure 9a, liquidus, Figure 10a, solidus) will be presented in detail. The aim of this part of the work is to study the effect of the number of data that came from the data of the liquidus and solidus surfaces (from the isotherms). In Table 13, the used isotherms and the number of data used in the calculations are shown. In the case of the third and fourth estimation, the total number of the used data is 279 and 938, respectively.

In the case of the liquidus, the form of the function of DELTA T as a function of the Cu concentration is similar to that of the second estimation in both cases (Figures 7b and 9b). In the case of the third estimation, the DELTA T_{max} and DELTA T_{aver} are less than those in the case of the second estimation. Considering the 14 isotherms, DELTA T_{max} and DELTA T_{aver} are less than 0.49 K and 0.44 K, respectively, except at the first isotherm, where those are 0.82 K and 0.77 K, respectively (Appendix A, Figure 17).

In the case of the solidus temperature, used only 1 isotherm, the DELTA T_{max} and DELTA T_{aver} are less than 1 K, except near the ternary eutectic point (810 K and 800 K), where those are 1.94 K and 1,65 K, respectively (Figure 7b). Used all 14 isotherms for the calculation DELTA T_{max} and DELTA $T_{aver,}$ less than 0.63 and 0.34 K, respectively (Appendix B, Figure 18).

The beginning temperature of solidification for binary eutectics can be calculated, as binary eutectic valleys are known in this case.

The error in the calculation can also be characterised by the difference between all the data calculated by ESTPHAD and Thermo-Calc (DELTA T*aver in Table 13).

Figure 19a,b show Delta T*aver (DELTA T*aver is the average of one type of estimation) as a function of data number in the case of liquidus and solidus temperature. It can be clearly seen that the DELTA T*aver drastically decreases with an increase in the number of data used for estimation (see the number of data in Table 13).

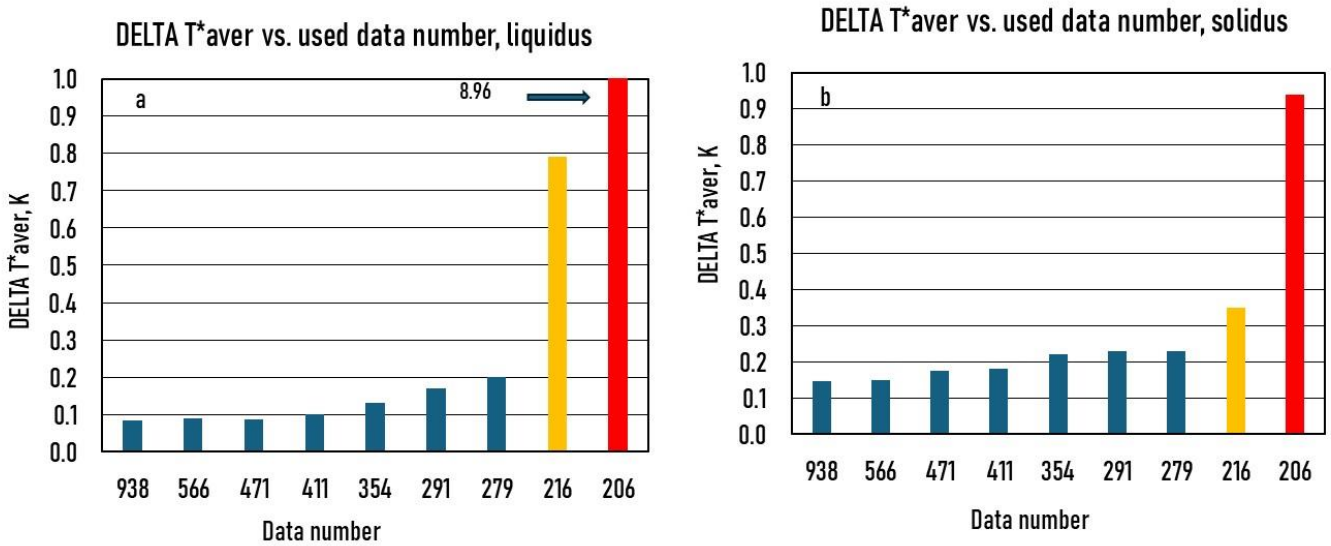


Figure 19. The temperature difference between the Thermo-Calc and ESTPAD as a function of data number. (**a**): liquidus, (**b**): solidus.

5.3. Calculation of the Beginning Temperature (T_{BE}) of Solidification of Binary Eutectics

Figure 11a shows the comparison of the ESTPHAD and Thermo-Calc calculations. The Surface 1 and Surface 2 show the beginning temperature of solidification for α+Si

and α+Al_2Cu binary eutectics, respectively. In Figure 11b, the calculated results of the ESTPHAD and Thermo-Calc are compared. It can be seen that the fit is acceptable (R^2~1). This fact proves that the assumption that the tie lines intersect each other at the origin was correct.

5.4. Liquidus Slopes

Figure 12 shows the calculated two liquidus slopes along the isotherms. The absolute value of the $\partial T_L/\partial X_{Si}$ continuously increases (Figure 12a), while the absolute value of $\partial T_L/\partial X_{Cu}$ decreases (Figure 12b) with the increase in Cu and Si concentration, respectively. Both values increase as the temperature decreases.

5.5. Some Examples

In Figure 11a, four compositions are selected to show the capability of the ESTPHAD method. The solidification processes in the case of the selected alloys are as follows:

Example 1
$T_L \rightarrow T_s$: liq$\rightarrow\alpha$
Example 2
$T_L \rightarrow T_{BE}$: liq$\rightarrow\alpha$
$T_{BE} \rightarrow T_{TE}$: liq$\rightarrow$($\alpha$+Si) (Surface 1)
T_{TE}: liq$\rightarrow$(α+Si+Al_2Cu)
Example 3
$T_L \rightarrow T_{BE}$: liq$\rightarrow\alpha$
$T_{BE} \rightarrow T_{TE}$: liq$\rightarrow$($\alpha$+$Al_2Cu$) (Surface 2)
T_{TE}: liq$\rightarrow\alpha$+Si+Al_2Cu
Example 4
$T_L \rightarrow T_{TE}$: liq$\rightarrow\alpha$
T_{TE}: liq$\rightarrow$(α+Si+Al_2Cu)
Table 15 shows the calculated results.

Table 15. The calculated liquidus, solidus, binary and ternary eutectic temperatures, liquidus slopes, and partition ratios.

	C_{Cu}, wt%	C_{Si}, wt%	T_L, K	T_s, K	T_{BE}, K	T_{TE}, K	Slope 1, K/wt% Si	Slope 2, K/wt% Cu	k_{Cu}	k_{Si}
Example 1	3	0.6	921.8	835.3	-	-	−6.01	−2.72	0.10	0.10
Example 2	10	7	856.6	-	825.4	798.5	−7.75	−3.62	0.12	0.12
Example 3	25	3	830.4	-	802,3	798.5	−9.18	−4.42	0.15	0.15
Example 4	18.48	3.54	852.6	-	-	798.5	−8.25	−3.86	0.13	0.13

5.6. Recalculation of the Solidus Isotherm from the Liquidus Isotherms Using the Partition Ratios

The error of the calculation of the partition ratios can be characterised by the maximum DELTA Cu_{max}, DELTA Si_{max}, and average DELTA Cu_{aver}, DELTA Si_{aver}. Both methods are used below. The values of the partition ratios are used in the simulation of solidification; in practice, those are less interesting. The important data are the starting and ending temperatures of solidification. The simulation results can be validated by comparing them with the measured concentration distribution. Therefore, the minimum concentration reliably measurable with the microprobe is used as a measure of usability, which is approximately 0.1 wt%. Thus, in the case of different estimates, this value is used when evaluating them.

The results of the four estimations are in Appendix A, and they are compared in Figures 20 and 21.

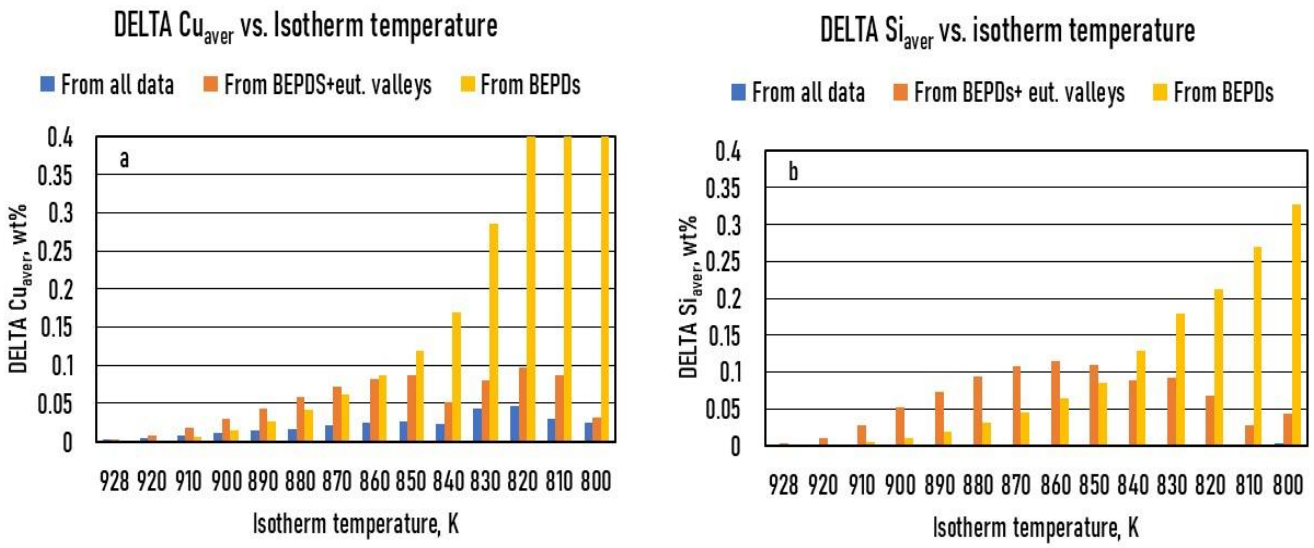


Figure 20. The maximum difference between the calculated and recalculated concentrations at three different estimations as a function of the isotherm temperatures (**a**) DELTA Cu_{max}, (**b**) DELTA Si_{max}.

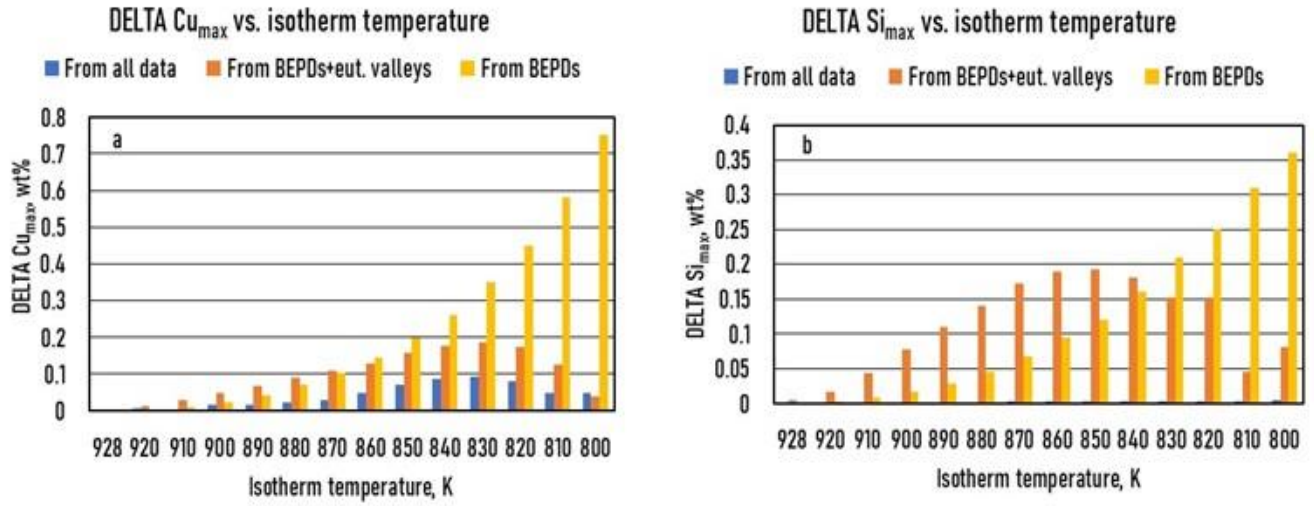


Figure 21. The average difference between the calculated and recalculated concentrations at three different estimations as a function of the isotherm temperatures. (**a**) DELTA Cu_{aver}, (**b**) DELTA Si_{aver}.

5.6.1. First Estimation

The partition ratios were calculated from the data of the two BEPDs. The results of the recalculated solidus isotherms are in Figure 14a. The isotherm start from one BEPD (e.g., Al-Cu), both types of DELTA Cu and DELTA Si along the isotherms continuously increase to a maximum (DELTA Cu_{max} and DELTA Si_{max}), then decrease to the other BEPD (Al-Si) (Figure 14b). In the case when the isotherm is not between two BEPS, the value of DELTA Cu_{max} and DELTA Si_{max} increases significantly, at 800 K are 0.78 wt% and 0.36 wt%. At 870 K, the DELTA Cu_{max} and DELTA Si_{max} are 0.103 wt% and 0.068 wt%. Thus, for alloys whose concentration is between the pour Al melting temperature (933 K) and the 870 K liquidus isotherm, the first estimation can be used in the simulation. Since the DELTA Cu_{aver} and DELTA Si_{aver} are less than the maximum at 860 K (0.086 wt% and 0.0631 wt%), considering the average, the limit is 860 K (Figure 16).

5.6.2. Second Estimation

The partition ratios were calculated from the data of the two BEPDs and the binary eutectics valleys. The results of the recalculated solidus isotherms are in Figure 15a. Along the isotherms, DELTA Cu and DELTA Si change similarly to the first estimation, but those are a little bit higher as in the case of the first estimation until 860 K (Figure 15b). The explanation for this is that, considering the data of binary eutectic valleys, somewhat worsens the precision of the calculation in the case of isotherms close to the Al corner, while the accuracy increases significantly near the ternary eutectic point.

Considering the average condition, the limit is achieved across the entire concentration range (Figure 16).

5.6.3. Third Estimation

This type of recalculation was not investigated.

5.6.4. Fourth Estimation

The partition ratios were calculated from the data of the two BEPDs, the binary eutectics valleys and all 14 isotherms. The results of the recalculated solidus isotherms are in Figure 16a. Along the isotherms calculated by partition ratios, DELTA Cu and DELTA Si change, a little confusing, but the DELTA Cu_{max} and DELTA Si_{max} are smaller as in the case of the second estimation (Figure 16b).

DELTA Cu and DELTA Si are less than 0.1 wt% for both conditions in the entire concentration range.

6. Summary

In the previous two articles [31,32], we presented the principle of the Estimation of Phase Diagram (ESTPHAD) calculation method for binary and ternary equilibrium phase diagrams. The usability of the method was demonstrated in the case of binary and ternary isomorphic and binary eutectic equilibrium phase diagrams. In this article, we describe the calculation procedure of the liquidus, solidus, initial temperature of the solidification of the binary eutectic, and the partition ratios in the case of the Al-Si-Cu eutectic ternary equilibrium phase diagrams. For the calculations, a database created with the Thermo-Calc software was used. Using four types of estimations, it has been shown that the error of each approximation. Based on the magnitude of the errors, the concentration range of the alloys has been determined, where the maximum and average error are less than 1 K for temperatures and less than 0.1 wt% for concentrations.

The partition ratios of Al-Si-Cu TEPD were calculated with three different estimations at the Al corner, where solidification begins with an Al solid solution. Using these partition ratios, the solidus concentrations were recalculated from the liquidus concentrations along the isotherms. Maximum and average errors were determined along the isotherms. Assuming that an error of 0.1 wt% Cu and Si % in the recalculated concentration (compared with the concentration of calculated solidus isotherms) is sufficient not only for practice but also for solidification simulations

It was found that,

(i) In a limited alloying concentration range, around the Al corner (bounded by an isotherm), the liquidus and solidus temperatures of the solid solution of the Al-Si-Cu ternary alloy can be calculated based on the liquidus and solidus of the binary Al-Si and Al-Cu EPD with an accuracy of 1K (first estimation). The concentration range bounded by an isotherm on the solidus surface is much smaller than the concentration range on

the liquidus surface bounded by the same isotherm. This estimation procedure can be used in cases of another TEPD, too, where only the two BEEPDs are known.

If only the two partition ratios are known from measured or calculated BEPD, the first estimation can be used in a relatively narrow concentration range, near the Al corner.

(ii) In many cases, binary eutectic valleys are known to enclose the solid solution in addition to BEPDs, and by using the temperature-concentration data of those, the liquidus and solidus temperatures of the solid solution can be calculated with an accuracy of 2 K in the concentration range enclosed by the eutectic valleys (second estimation). Knowing the eutectic valleys on the liquidus and the solidus surfaces, the beginning temperature of solidification for binary eutectics can also be calculated. These results are already acceptable for practical purposes.

The second estimation can be used in a smaller concentration range than the first estimation near the Al corner, using the maximum error condition. Considering the average condition, the limit is achieved in the entire concentration range.

(iii) Knowing data on the liquidus and solidus surfaces, the accuracy drastically increases (less than 1 K) (third estimation). By using a large amount of data (~1000) (fourth estimation), the accuracy can be further increased (ΔT^*_{aver} liquidus: 0.083 K, solidus: 0.147 K), and the calculated temperatures are suitable for simulations.

The fourth estimation for partition ratios can be used across the entire concentration range, considering both maximum and average conditions; the limit is achieved throughout the entire concentration range. It is worth noting that the correct partition ratios are only known from the calculated TEPD.

However, it should be noted that the error of the result of ESTPHAD (the difference between the measured or calculated by Thermo-Calc values and the calculated values of ESTPHAD) strongly depends on the accuracy of the measuring or the Thermo-Calc calculation.

Key benefits of the ESTPHAD Method:

(i) The equations used to calculate the liquidus and solidus temperatures and the partition quotients are developed on a thermodynamic basis, against other approximation procedures;

(ii) The constants of the equations can be calculated directly from the measured results of the liquidus and solidus temperatures or from the data obtained by digitising graphically known diagrams, even with EXCEL, and no other software is required;

(iii) The constants of the equations can be calculated from results calculated by a Calphad-type software;

(iv) The use of equations speeds up the simulation of solidification by several orders of magnitude with the same accuracy as the Calphad-type software.

Author Contributions: Conceptualization, A.R.; methodology, G.K. and Á.V.; software, G.K. and Á.V.; validation, G.K. and Á.V.; formal analysis, G.K. and Á.V.; investigation, G.K.; resources, A.R., T.M. and Á.V.; data curation, A.R., T.M. and Á.V.; writing—original draft preparation, G.K. and T.M.; writing—review and editing, A.R. All authors have read and agreed to the published version of the manuscript.

Funding: This research was funded by the European Space Agency under the CETSOL/HUNGARY ESA PRODEX (No. 4000131880/NL/SH) projects.

Data Availability Statement: The original contributions presented in this study are included in the article. Further inquiries can be directed to the corresponding author.

Conflicts of Interest: The authors declare no conflicts of interest.

Abbreviations

Acronim	
CALPHAD	CALculation of PHAse Diagram
ESTPHAD	ESTimation of PHAse Diagram
EPD	equilibrium phase diagram
BEPD	binary equilibrium phase diagram
TEPD	ternary equilibrium phase diagram
Symbols	
G	free energy of alloy
$\mu_A,\ \mu_B, \mu_C$	chemical potential
$G_A,\ G_B$	free energy of A and B elements
G_A^l, G_C^l	free energy of A and B elements in the liquid phase
G_A^s, G_B^s	free energy of A and B elements in the solid phase
X_A, X_B	concentration of A and B elements of the alloy
$X_{Si}^l, X,_{Cu}^l$	concentration of Si, and Cu elements in the liquid phase
$X_{Si}^s X,_{Cu}^s$	concentrations of Si, and Cu elements in the solid phase
μ_A^l, μ_B^l	partial molar free energy of A and B elements in the liquid phase
μ_A^s, μ_B^s	partial molar free energy of A and B elements in solid phase
Ω^l *and* Ω^s	interaction parameter in liquid and solid őhases
T	absolute temperature
T_{Al}	melting point of pure Aluminium
$T_L\left(X_{Si}^l, X_{Cu}^l\right)$	liquidus and solidus temperature of the A-B-C TEPD
R	gas constant
k_{Si}^{AlSi}, k_{Cu}^{AlCu}	partition ratio of Si and Cu elements in the Al-Si and Al-Cu alloy
k_{Si}^{AlSiCu}, and k_{Cu}^{AlSiCu}	partition ratio of Si and Cu elements in the Al-Si-Cu alloy
M_{AlSiCu}^{Si}, M_{AlSiCu}^{Cu}	liquidus slope in Al-Si-Cu TEPD
$S_{AlSiCu}^l\left(X_{Si}^l, X_{Cu}^l\right)$	numerator in the case of the slope calculation,
$F_{AlSi}^l\left(X_{Si}^l\right), F_{AlCu}^l\left(X_{Cu}^l\right)$ and	maps for the calculation of the $\boldsymbol{F_{AlSi}^l}\left(X_{Si}^l\right)$, $\boldsymbol{F_{AlSi}^s}(X_{Si}^s)$ and
and $F_{AlSi}^s(X_{Si}^s), F_{AlCu}^s(X_{Cu}^s)$	and $\boldsymbol{F_{AlCu}^l}\left(X_{Cu}^l\right)$, $\boldsymbol{F_{AlCu}^s}(X_{Cu}^s)$ functions
$F_{AlSiCu}^l\left(X_{Si}^l, X_{Cu}^l\right)$, and $F_{AlSiCu}^s(X_B^s, X_C^s)$	map for the calculation of the $\boldsymbol{F_{AlSiCu}^l}\left(X_{Si}^l, X_C^{lu}\right)$ *and* $\boldsymbol{F_{AlSiCu}^s}(X_{Si}^s, X_{Cu}^s)$ functions
$\Delta F_{AlSiCu}^l\left(X_{Si}^l, X_C^l u\right)$, and $\Delta F_{AlSiCu}^s(X_B^s, X_C^s)$	map for the calculation of the $\boldsymbol{\Delta F_{AlSiCu}^l}\left(X_{Si}^l, X_{Cu}^l\right)$ *and* $\boldsymbol{\Delta F_{AlSiCu}^s}(X_{Si}^s, X_{Cu}^s)$ functions
$A_{AlSi}^l(i)$ and $A_{AlSi}^s(i)$	constants of the $\boldsymbol{F_{AlSi}^l}\left(X_{Si}^l\right)$ and $\boldsymbol{F_{AlSi}^s}(X_{Si}^s)$ functions
$A_{AlCu}^l(i)$ and $A_{AlCu}^s(i)$	constants of the $\boldsymbol{F_{AlCu}^l}\left(X_{Cu}^l\right)$ and $\boldsymbol{F_{AlCu}^s}(X_{Cu}^s)$ functions
A_{AlSiCu}^l(i) and $A_{AlSiCu}^s(i)$	constants of the $\boldsymbol{\Delta F_{AlSiCu}^l}\left(Si, X_{Cu}^l\right)$ *and* $\boldsymbol{\Delta F_{AlSiCu}^s}(X_{Si}^s, X_{Cu}^s)$ functions
$lnk_{Si}^{AlSi}\left(X_{Si}^l\right)$ $lnk_C^{AC}\left(X_C^l\right)$,	maps for the calculation of the $\boldsymbol{lnk_{Si}^{AlSi}}\left(\boldsymbol{X_{Si}^l}\right)$, and $\boldsymbol{lnk_{Cu}^{AlCu}}\left(\boldsymbol{X_C^l}\right)$, functions
$B_{AB}^l(i)$ *and* $B_{AB}^s(i)$	constants of the $\boldsymbol{lnk_{Si}^{AlSi}}\left(X_{Si}^l\right)$
$B_{AC}^l(i)$ *and* $B_{AC}^s(i)$	constants of the $\boldsymbol{lnk_{Cu}^{AlCu}}\left(X_{Cu}^l\right)$
$\Delta lnk_{Si}^{AlSiCu}\left(X_{Si}^l, X_{Cu}^l\right)$, $\Delta lnk_{Cu}^{AlSiCu}\left(X_{Si}^l, X_{Cu}^l\right)$	maps for the calculation of the $\boldsymbol{\Delta lnk_{Si}^{AlSiCu}}\left(X_{Si}^l, X_{Cu}^l\right)$ and $\boldsymbol{\Delta lnk_{Cu}^{AlSiCu}}\left(X_{Si}^l, X_{Cu}^l\right)$
$B_{AlSiCu}^l(i)$	constants of the $\boldsymbol{\Delta lnk_B^{AlSiCu}}\left(X_{Si}^l, X_{Cu}^l\right)$ functions
$C_{AlSiCu}^l(i)$	constants of the $\boldsymbol{\Delta lnk_C^{AlSiCu}}\left(X_{Si}^l, X_{Cu}^l\right)$ functions
Subscripts	
m, i	number ofconstants
Superscripts	
l, s	liquid, solid

Appendix A

Table A1. The liquidus temperature difference between the Thermo-Calc and ESTPHAD calculations at four different estimations as a function of the isotherm temperatures. a: average, b: maximum.

a	**DELTA T_{aver} vs. Liquidus Isotherm**			
T, K	Fourth est.	Third est.	Second est.	First est.
928	0.75	0.75	0.78	0.73
920	0.17	0.17	0.29	0.07
910	0.12	0.14	0.48	0.32
900	0.06	0.08	0.65	0.92
890	0.07	0.08	0.83	1.77
880	0.09	0.09	0.99	2.81
870	0.08	0.08	1.09	4.02
860	0.05	0.07	1.13	5.41
850	0.06	0.08	1.08	6.97
840	0.05	0.1	0.69	10.14
830	0.06	0.05	0.88	13.95
820	0.08	0.08	0.74	15.94
810	0.04	0.21	0.31	19.27
800	0.13	0.44	0.45	22.18
b	**DELTA T_{max} vs. liquidus isotherm**			
T, K	Fourth est.	Third est.	Second est.	First est.
928	0.82	0.82	0.83	0.82
920	0.27	0.27	0.42	0.27
910	0.16	0.19	0.72	0.51
900	0.09	0.14	1.04	1.42
890	0.19	0.19	1.34	2.69
880	0.18	0.18	1.61	4.28
870	0.14	0.13	1.82	6.18
860	0.1	0.13	1.95	8.37
850	0.19	0.19	1.98	10.8
840	0.25	0.2	1.87	13.49
830	0.25	0.14	1.6	16.4
820	0.35	0.36	1.15	19.51
810	0.14	0.33	0.48	22.71
800	0.18	0.49	0.59	24.73

Appendix B

Table A2. The solidus temperature difference between the Thermo-Calc and ESTPHAD calculations at four different estimations as a function of the isotherm temperatures. a: average, b: maximum.

a	**DELTA T_{aver} vs. Solidus Isotherm**			
T, K	Fourth est.	Third est.	Second est.	First est.
928	0.67	0.67	0.67	0.66
920	0.05	0.06	0.04	0.02
910	0.03	0.07	0.02	0.07
900	0.02	0.06	0.07	0.18
890	0.05	0.06	0.14	0.29
880	0.09	0.06	0.21	0.39
870	0.1	0.08	0.26	0.45
860	0.1	0.09	0.27	0.44
850	0.1	0.11	0.26	0.40
840	0.16	0.09	0.17	0.61
830	0.12	0.08	0.22	0.5
820	0.18	0.11	0.4	1.27
810	0.17	0.59	0.8	2.66
800	0.34	1.65	1.6	4.23

Table A2. *Cont.*

b	DELTA T_{max} vs. solidus isotherm			
T, K	Fourth est.	Third est.	Second est.	First est.
928	0.71	0.71	0.7	0.7
920	0.06	0.06	0.06	0.058
910	0.06	0.08	0.06	0.13
900	0.04	0.09	0.11	0.29
890	0.1	0.1	0.2	0.46
880	0.16	0.12	0.29	0.62
870	0.2	0.15	0.35	0.75
860	0.22	0.19	0.39	0.83
850	0.23	0.23	0.42	0.84
840	0.2	0.23	0.46	0.8
830	0.25	0.16	0.56	1.15
820	0.27	0.22	0.83	1.96
810	0.36	0.97	1.56	3.01
800	0.63	1.94	2.1	4.31

Appendix C

Table A3. The maximum difference between the calculated and recalculated concentrations at three different estimations as a function of the isotherm temperatures. a. DELTA Cumax, b: DELTA Simax.

a	DELTA Cu_{max}, wt%		
T, K	Fourth est.	Second est.	First est.
928	0.0028	0.004	0.0017
920	0.0069	0.0129	0.0011
910	0.0013	0.0293	0.0100
900	0.0188	0.0487	0.0237
890	0.0227	0.0690	0.043
880	0.0236	0.0893	0.07
870	0.0288	0.1103	0.103
860	0.0493	0.1336	0.147
850	0.0713	0.1582	0.2
840	0.0878	0.1786	0.27
830	0.0936	0.1870	0.35
820	0.1438	0.1736	0.45
810	0.0548	0.1278	0.59
800	0.047	0.04	0.78
b	**DELTA Si_{max}, wt%**		
T, K	Fourth est.	Second est.	First est.
928	0.0002	0.0039	0.0005
920	0.0003	0.0166	0.0023
910	0.0007	0.0441	0.0073
900	0.0012	0.0776	0.0163
890	0.0017	0.1135	0.029
880	0.0022	0.1465	0.046
870	0.0027	0.1729	0.068
860	0.003	0.19	0.095
850	0.0031	0.1926	0.12
840	0.0029	0.1808	0.17
830	0.0024	0.1526	0.21
820	0.0030	0.1076	0.26
810	0.0033	0.0461	0.31
800	0.0044	0.08	0.36

Appendix D

Table A4. The absolute average difference between the calculated and recalculated concentrations at three different estimations as a function of the isotherm temperatures. a. DELTA Cu_{aver}, b: DELTA $Si_{aver.}$

a	**DELTA Cu_{aver}, wt%**		
T, K	Fourth est.	Second est.	First est.
928	0.002	0.0027	0.0012
920	0.0041	0.0077	0.0006
910	0.008	0.0181	0.0054
900	0.0115	0.0303	0.0144
890	0.014	0.044	0.0265
880	0.0167	0.058	0.0414
870	0.021	0.0716	0.0609
860	0.0247	0.0821	0.086
850	0.026	0.0869	0.1178
840	0.0235	0.0519	0.17
830	0.0428	0.0804	0.2851
820	0.0472	0.0976	0.4015
810	0.0295	0.087	0.57
800	0.0244	0.032	0.7757
T, K	DELTA Si_{aver}, wt%		
b	Fourth est.	Second est.	First est.
928	0.0002	0.0024	0.0004
920	0.0002	0.01	0.0014
910	0.0004	0.0282	0.0048
900	0.0007	0.0497	0.0104
890	0.0009	0.0731	0.0191
880	0.001	0.0934	0.0305
870	0.0012	0.1086	0.0451
860	0.0013	0.1152	0.0631
850	0.0014	0.1096	0.0845
840	0.0018	0.0883	0.1289
830	0.0012	0.0927	0.1799
820	0.002	0.0672	0.2133
810	0.0019	0.0283	0.2704
800	0.0024	0.0438	0.3265

References

1. Roósz, A.; Exner, H.E. Ternary restricted-equilibrium phase diagram-I. A first report: General principles and definitions. *Acta Metall. Mater.* **1990**, *38*, 2003–2008. [CrossRef]
2. Roósz, A.; Exner, H.E. Ternary restricted-equilibrium phase diagram-II. Practical application: Aluminium-rich corner of the Al-Cu-Mg system. *Acta Metall. Mater.* **1990**, *38*, 2009–2016. [CrossRef]
3. Kaufman, L.; Bernstein, H. *Computer Calculation of Phase Diagrams*; Academic Press: New York, NY, USA, 1970.
4. Kuz, W.; Fisher, D.J. *Fundamentals of Solidification*, 3rd ed.; Trans. Tech. Publications: Bäch, Switzerland, 1992.
5. Danntzig, J.A.; Rappaz, M. *Solidification Engineering Science, Materials*; EPFL Press: Lausanne, Switzerland, 2009.
6. Zhao, G.; Li, X.Z.; Xu, D.; Guo, J.; Fu, H.; Du, Y.; He, Y. Numerical Computations for Temperature, fraction of Solid Phase and Composition coupling in Ternary Alloy Solidification with Three Different Thermodynamic Data-acquisition Method. *Calphad* **2012**, *36*, 155–162. [CrossRef]
7. Djurdjevic, M.B.; Manasijevic, A.; Odonovic, Z.; Dolic, N. Calculation of Liquidus Temperature for Aluminium and Magnesium alloys Applying Method of Equivalency. *Adv. Mater. Sci. Eng.* **2013**, *2013*, 170527. [CrossRef]
8. Robles Hernandez, F.C.; Djurdjevic, M.B.; Kierkus, W.T.; Sokolowski, J.H. Calculation of the liquidus temperature for hypo and hypereutectic aluminium silicon alloys. *Mater. Sci. Eng. A* **2005**, *396*, 271–276. [CrossRef]
9. Farahany, S.; Erfani, M.; Karamoozia, A.; Ourdjini, A.; Idris, M.H. Artificial Neural Networks to Predict of Liquidus Temperature in Hypoeutectic Al-Si Cast Alloys. *J. Appl. Sci.* **2010**, *10*, 3243–3249. [CrossRef]

10. Wang, X.; Wang, X.; Wang, B.; Wang, B.; Liu, Q. Differential Calculation Model for Liquidus Temperature of Steel. *Steel Res. Int.* **2011**, *82*, 164–168. [CrossRef]
11. Min, L.; Hongbo, L.; Rongyuan, X.; Xiaorui, C.; Ying, L.; Hao, X.; Caidong, Z.; Zhiqiang, T. Investigation of the liquidus temperature calculation method for medium manganese steel. *High Temp. Mater. Process.* **2023**, *42*, 20220285. [CrossRef]
12. Sertucha, J.; Lacaze, J.; Regordosa, A.; Suarez, R. Polynomial Description of the Fe–C–Si Stable Phase Diagram for up to 4.5 Wt% Si, Including the Effect of Cr, Cu, Mn and P. *Int. J. Met.* **2025**, *19*, 1847–1856. [CrossRef]
13. Vorozhtcov, V.A.; Pavelina, M.E.; Stolyarova, V.L.; Fedorova, A.V.; Sinelshchikova, O.Y.; Almjashev, V.I. Liquidus temperatures in the La_2O_3-SrO-TiO_2-ZrO_2-Fe_2O_3 system: Calculation and experiment. *Ceram. Int.* **2025**, *51*, 320–330. [CrossRef]
14. Afanasyev, O.S.; Afanasyeva, E.A.; Egorov, G.F. Analytical Approximation and Numerical Simulation of Liquid for Nonequilibrium Multicomponent Eutectic Systems. *Vestn. Samara State Tech. Univ. Tech. Sci. Ser.* **2022**, *30*, 6–19. [CrossRef]
15. Zhang, Y.; Hu, B.; Zeng, G.; Liu, S.; Du, Y.; Yin, H. Experimental investigation, thermodynamic modelling and solidified microstructure of the Cu–Ti–Nb ternary system. *Calphad* **2022**, *76*. [CrossRef]
16. Jin, C.; Hu, B.; Zeng, G.; Xie, J.; Sheng, S.; Liu, S.; Hu, J. Experimental investigation and CALPHAD modelling of phase equilibria of the Cu–Ag–Zr system. *Calphad* **2022**, *79*, 102487. [CrossRef]
17. Zhang, Y.; Hu, B.; Li, B.; Zhang, M.; Wang, Q.; Du, Y. Experimental investigation and CALPHAD modelling of the Cu–Cr–Si ternary system. *Calphad* **2021**, *74*, 102324. [CrossRef]
18. Zhou, J.-Q.; Hu, B.; Li, B.-F.; Du, Y.; Wang, J. Experimental investigation and thermodynamic modelling of Cu–Nb–Si system. *Trans. Nonferrous Met. Soc. China* **2023**, *33*, 824−838. [CrossRef]
19. Ferreira, I.L.; Garcia, A.; Nestler, B. On macrosegregation in ternary Al-Cu-Si alloys: Numerical and experimental analysis. *Scr. Mater.* **2004**, *50*, 407–411. [CrossRef]
20. Du, Q.; Eskin, D.G.; Katgerman, L. Modeling Macrosegregation during Direct-Chill Casting of Multicomponent Aluminium Alloys. *Metall. Mater. Trans. A* **2007**, *38*, 180–189. [CrossRef]
21. Zhang, C.; Miao, J.; Chen, S.; Zhang, F.; Luo, A.A. CALPHAD-Based Modelling and Experimental Validation of Microstructural Evaluation and Microsegregation in Magnesium Alloys During Solidification. *J. Phase Equilib. Diffus.* **2019**, *40*, 495–507. [CrossRef]
22. Mikolajczak, P.; Geanau, A.; Ratke, L. Mushy Zone Calculation with Application of CALPHAD Technique. *Metals* **2017**, *7*, 363. [CrossRef]
23. Grafe, U.; Böttger, B.; Tiaden, J.; Fries, S.G. Coupling of Multicomponent Thermodynamic Databases to a Phase Field Model: Application to Solidification and Solid State Transformations of Superalloys. *Scr. Mater.* **2000**, *42*, 1179–1186. [CrossRef]
24. Kattner, U. The Thermodynamic Modelling of Multicomponent Phase Equilibria. *JOM* **1997**, *49*, 14–19. [CrossRef]
25. Greven, K.; Ludwig, A.; Hofmeister, T.; Sahm, R.R. *Solidification of Metallic Melts in Research and Technology*; Ludwig, A., Ed.; Wiley VCH: Weinheim, Germany, 1999; p. 119.
26. Dore, X.; Combeau, H.; Rappaz, M. Modelling of microsegregation in ternary alloys: Application to the solidification of Al–Mg–Si. *Acta. Mater.* **2000**, *48*, 3951–3962. [CrossRef]
27. Du, Q.; Eskin, D.G.; Katgerman, L. An efficient technique for describing a multi-component open system solidification path. *Comput. Coupling Phase Diagr. Thermochem.* **2008**, *32*, 478–484. [CrossRef]
28. Zhao, G.; Xu, D.; Fu, H. Thermo-Calc-based numerical computations for temperature, fraction of solid phase and composition couplings in alloy solidification. *Int. J. Mater. Res.* **2008**, *99*, 680–688. [CrossRef]
29. Qiu, K.; Wang, R.C.; Peng, C.Q. Mathematical model of Liquidus Temperature in Quaternary Aluminium Phase Diagram. *Adv. Mater. Res.* **2015**, *1095*, 545–548. [CrossRef]
30. Qiu, K.; Wang, R.; Peng, C.; Lu, X.; Wang, N. Polynomial regression and interpolation of thermodynamic data in Al-Si-Mg-Fe system. *Comput. Coupling Phase Diagr. Thermochem.* **2015**, *48*, 175–183. [CrossRef]
31. Kőrösy, G.; Roósz, A.; Mende, T. The ESTPHAD Concept: An Optimised Set of Simplified equations to Estimate the Equilibrium Liquidus and Solidus Temperatures, Partition Ratio and Liquidus Slope for Quick Access to Equilibrium Data in Solidification Software, Part I: Binary equilibrium phase diagram. *Metals* **2024**, *14*, 1266.
32. Kőrösy, G.; Roósz, A.; Mende, T. An Optimised Set of Simplified equations to Estimate the Equilibrium Liquidus and Solidus Temperatures, Partition Ratio and Liquidus Slope for Quick Access to Equilibrium Data in Solidification Software, Part II, Ternarx Isomorphous Equilibrium Phase Diagram. *Metals* **2025**, *15*, 803.

Disclaimer/Publisher's Note: The statements, opinions and data contained in all publications are solely those of the individual author(s) and contributor(s) and not of MDPI and/or the editor(s). MDPI and/or the editor(s) disclaim responsibility for any injury to people or property resulting from any ideas, methods, instructions or products referred to in the content.